

Signal Models

2.1 Components of a Radar Signal

While a radar transmits a controlled, well-defined signal, the signal measured at the receiver output in response is the superposition of several major components, none of them entirely under the control of the designer. The major components are the *target*, *clutter*, *noise*, and, in some cases, *jamming*. These signals are sometimes subdivided further. For instance, clutter can be separated into ground clutter and weather clutter (such as rain), while jamming can be separated into active jamming (noise transmitters) and passive jamming (such as chaff clouds). Signal processing is applied to this composite signal; the goal is to extract useful information regarding the presence of targets and their characteristics, or to form a radar image. Noise and jamming are interference signals; they degrade the ability to measure targets. Clutter may be interference in some cases, such as detecting aircraft, or may be the desired signal itself, as with a ground imaging radar. The effectiveness of the signal processing is measured by the improvement it provides in the various figures of merit discussed in Chap. 1, such as detection probability, *signal-to-interference ratio* (SIR), or angle accuracy.

It was shown in Chap. 1 that conventional pulsed radars transmit narrowband, bandpass signals. Transmitted energy is maximized by restricting amplitude modulation to on-off pulsing; phase modulation is used to expand the instantaneous bandwidth when needed to improve resolution. Thus, an individual transmitted radar pulse can be written as

$$\bar{x}(t) = a(t) \sin[2\pi F_t t + \theta(t)] \quad (2.1)$$

where $a(t)$ is the constant amplitude pulse envelope, F_t is the radar carrier frequency, and $\theta(t)$ may be a constant or may represent phase modulation of the pulse. It will usually be assumed that $a(t)$ is an ideal, square pulse envelope of amplitude A and duration τ seconds. The instantaneous power

of this signal is just $P_s = A^2/2$. The signal at the receiver output will be a combination of echoes of $\tilde{x}(t)$ from targets and clutter, noise, and possibly jamming.

Because the target and clutter components are delayed echoes of the transmitted pulse, they are also narrowband signals, although their amplitude and phase modulation will in general be altered, e.g., by propagation loss and Doppler shift. Receiver noise appears as an additive random signal. Thus, the received signal resulting from a single pulse echoing from a scatterer at range $R_0 = ct_0/2$ can be modeled as

$$\bar{y}(t) = b(t - t_0)e^{j[2\pi F_t(t-t_0)+\phi(t)]} + n(t) \quad (2.2)$$

where $n(t)$ = receiver noise

$b(t)$ = echo amplitude

$\phi(t)$ = echo phase modulation.

The important parameters of $\bar{y}(t)$ are the delay time t_0 , echo component amplitude $b(t)$, its power relative to the noise component, and the echo phase modulation function $\phi(t)$. These characteristics are used to estimate target range, scattering strength, and radial velocity.

The amplitude and phase modulation functions also determine the range resolution ΔR of a measurement. For example, $\Delta R = c\tau/2$ if $\theta(t)$ is a constant. Resolution in angle and cross-range is determined by the 3-dB width of the antenna pattern.

In order to design good signal processing algorithms, good models of the signals to be processed are needed. In this chapter, an understanding of common radar signal characteristics pertinent to signal processing is developed by presenting models of the effect of the scattering process on the amplitude, phase, and resolution properties of radar measurements. While deterministic models suffice for simple scatterers, it will be seen that complicated real targets require statistical descriptions of the scattering process.

2.2 Amplitude Models

2.2.1 Simple point target radar range equation

The *radar range equation* (Eaves and Reedy, 1987; Skolnik, 2001) is a deterministic model that relates received echo power to transmitted power in terms of a variety of system design parameters. It is a fundamental relation used for basic system design and analysis. Since the received signals are narrowband pulses of the form of Eq. (2.2), the received power P_r estimated by the range equation can be directly related to the received pulse amplitude.

To derive the range equation, assume that an isotropic radiating element transmits a waveform of power P_t watts into a lossless medium. Because the transmission is isotropic and no power is lost in the medium, the power density at a range R is the total power P_t divided by the surface area of a sphere of

radius R , which is

$$\text{Isotropic transmitted power density} = \frac{P_t}{4\pi R^2} \quad \text{W/m}^2 \quad (2.3)$$

Of course, real radars use directive antennas to focus the outgoing energy, rather than isotropic radiators. As described in Chap. 1, the antenna gain G is the ratio of maximum power density to isotropic density. Thus, in the direction of maximum radiation intensity, the power density at range R becomes

$$\text{Peak transmitted power density} = Q_t = \frac{P_t G}{4\pi R^2} \quad \text{W/m}^2 \quad (2.4)$$

This is the power density incident upon the target if it is aligned with the antenna's axis of maximum gain.

When the electromagnetic wave with power density given by Eq. (2.4) is incident upon a single discrete scattering object, or *point target*, at range R the incident energy is scattered in various directions; some of it may also be absorbed by the scatterer itself. In particular, some of the incident power is reradiated, or *backscattered*, toward the radar. Imagine that the target collects all of the energy incident upon a collector of area σ square meters and reradiates it isotropically. The reradiated power is then

$$\text{Backscattered power} = P_b = \frac{P_t G \sigma}{4\pi R^2} \quad \text{W} \quad (2.5)$$

The quantity σ is called the *radar cross section* (RCS) of the target. One important fact about RCS is that σ is *not* equal to the physical cross-sectional area of the target; it is an equivalent area that can be used to relate incident power density at the target to the reflected power density that results at the receiver. RCS will be discussed further in Sec. 2.2.3.

Because RCS is defined under the assumption that the backscattered power is reradiated isotropically, the density of the backscattered power at a range R is found by dividing the power of Eq. (2.5) by the surface area of a sphere of radius R as was done in Eq. (2.3), giving the backscattered power density at the radar receiver as

$$\text{Backscattered power density} = Q_b = \frac{P_t G \sigma}{(4\pi)^2 R^4} \quad \text{W/m}^2 \quad (2.6)$$

If the effective aperture size of the radar antenna is A_e square meters, the total backscattered power collected by the receiving antenna will be

$$\text{Received power} = P_r = \frac{P_t G A_e \sigma}{(4\pi)^2 R^4} \quad \text{W} \quad (2.7)$$

It was shown in Chap. 1 that the effective aperture of an antenna is related to its gain and operating wavelength according to $A_e = \lambda^2 G / 4\pi$. Thus

$$P_r = \frac{P_t G^2 \lambda^2 \sigma}{(4\pi)^3 R^4} \quad \text{W} \quad (2.8)$$

Equation (2.8) describes the power that would be received if an ideal radar operated in free space and used no signal processing techniques to improve sensitivity. Various additional “loss” and “gain” factors are customarily added to the formula to account for a variety of additional considerations. For example, losses incurred in various components such as the duplexers, power dividers, waveguide, and radome (a protective covering over the antenna), and propagation effects not found in free space propagation, can be lumped into a *system loss factor* L_s that reduces the received power. System losses are typically in the range of 3 to 10 dB but can vary widely. One of the most important loss factors, particularly at X band and higher frequencies, is atmospheric attenuation $L_a(R)$. Unlike system losses, atmospheric losses are a function of range. If the one-way loss in decibels per kilometer of Fig. 1.3 is denoted by α , the loss in decibels for a target at range R meters (not kilometers) is

$$L_a(R)(\text{dB}) = 2\alpha(R/1000) = \alpha R/500 \quad (2.9)$$

In linear units, the loss is therefore

$$L_a(R) = 10^{\alpha R/5000} \quad (2.10)$$

Atmospheric loss can be inconsequential at 10 GHz and moderate ranges, or tens of decibels at 60 GHz and a range of a few kilometers (the reason why 60 GHz is not a popular radar frequency). This example also shows that, like system losses, atmospheric loss is a strong function of radar frequency.

Incorporating atmospheric and system losses in Eq. (2.8) finally gives

$$P_r = \frac{P_t G^2 \lambda^2 \sigma}{(4\pi)^3 R^4 L_s L_a(R)} \quad \text{W} \quad (2.11)$$

Equation (2.11) is one simple form of the *radar range equation*. It relates received echo power to fundamental radar system and target parameters such as transmitted power, operating frequency, and antenna gain; radar cross section; and range. Because the power of the radar signal is proportional to the square of the electric field amplitude, the range equation also serves as a model of the amplitude of the target and clutter components of the signal. Note that all variables in Eq. (2.11) are in linear units, not decibels, even though several of the parameters are often specified in decibels; frequent examples include the atmospheric losses, antenna gain, and RCS. Also note that P_r is instantaneous, not average, received power.

As an example, consider an X-band (10 GHz) radar with a peak transmitted power of 1 kW and a pencil beam antenna with a 1° beamwidth, and suppose an echo is received from a jumbo jet aircraft with an RCS of 100 m² at a range of 10 km. The received power can be determined using Eq. (2.11). The antenna gain can be estimated from Eq. (1.10) to be $G = 26,000/(1)(1) = 26,000 = 44$ dB. The wavelength is $\lambda = c/F = 3 \times 10^8/10 \times 10^9 = 3 \times 10^{-2}$ m = 3 cm.

Assuming atmospheric and system losses are negligible, the received power is

$$P_r = \frac{(1000)(26,000)^2(0.03)^2(100)}{(4\pi)^3(10,000)^4} = 3.066 \times 10^{-9} \quad \text{W} \quad (2.12)$$

The received power is only 1.8 nW, 12 orders of magnitude less than the transmitted power. Nonetheless, it will be seen that this signal level is adequate for reliable detection in many cases. This example illustrates the huge dynamic ranges observed in radar between transmitted and received signal powers.

An important consequence of Eq. (2.11) is that, for a point target, the received power decreases as the fourth power of range from the radar to the target. Thus, the ability to detect a target of a given radar cross section decreases rapidly with range. Range can be increased by increasing transmitted power, but because of the R^4 dependence, the power must be raised by a factor of 16 (12 dB) just to double the effective range. Alternatively, the antenna gain can be increased by a factor of 4 (6 dB), implying an increase in antenna area by a factor of 4. On the other hand, designers of “stealth” aircraft and other vehicles must reduce the RCS σ by a factor of 16 in order to halve the range at which they can be detected by a given radar system.

The range equation is a fundamental radar system design and analysis tool. More elaborate or specialized versions of the equation can be formulated to show the effect of other variables, such as pulse length, *intermediate frequency* (IF) bandwidth, or signal processing gains. The range equation also provides the basis for calibrating a radar system. If the system power, gain, and losses are carefully characterized, then the expected received power of echoes from test targets of known RCS can be computed. Calibration tables equating receiver voltage observed due to those same echoes to incident power density can then be constructed.

Signal processing techniques can increase the effective received power, and therefore increase the obtainable range. The effect of each technique on received power is discussed as they are introduced in later chapters.

2.2.2 Distributed target forms of the range equation

Not all scattering phenomena can be modeled as a reflection from a single point scatterer. Ground clutter, for example, is best modeled as distributed scattering from a surface, while meteorological phenomena such as rain or hail are modeled as distributed scattering from a three-dimensional volume. The radar range equation can be rederived in a generalized way that accommodates all three cases.

Equation (2.3) is still applicable as a starting point. To consider distributed scatterers, and because the gain of the antenna varies with azimuth and elevation angle, Eq. (2.4) must be replaced with an equation that accounts for the

effect of the antenna power pattern $P(\theta, \phi)$ on the power density radiated in a particular direction (θ, ϕ)

$$Q_t(\theta, \phi) = \frac{P_t P(\theta, \phi)}{4\pi R^2} \quad (2.13)$$

Assume that the antenna boresight corresponds to $\theta = \phi = 0$. The antenna boresight is normally the axis of maximum gain so that $P(0, 0) = G$.

Now consider the scattering from an incremental volume dV located at range and angle coordinates (R, θ, ϕ) . Suppose the incremental RCS of the volume element is $d\sigma$ square meters, and that $d\sigma$ in general varies with position in space. The incremental backscattered power from dV is

$$dP_b(\theta, \phi) = \frac{P_t P(\theta, \phi) d\sigma(R, \theta, \phi)}{4\pi R^2} \quad (2.14)$$

As before, $d\sigma$ is defined such that it is assumed this power is reradiated isotropically, and then collected by the antenna effective aperture, adjusted for the angle of arrival. After substituting for effective aperture and accounting for losses, this results in an incremental received power of

$$dP_r = \frac{P_t P^2(\theta, \phi) \lambda^2 d\sigma(R, \theta, \phi)}{(4\pi)^3 R^4 L_s L_a(R)} \quad (2.15)$$

The total received power is obtained by integrating over all space to obtain the *generalized radar range equation*

$$P_r = \frac{P_t \lambda^2}{(4\pi)^3 L_s} \int_V \frac{P^2(\theta, \phi)}{R^4 L_a(R)} d\sigma(R, \theta, \phi) \quad (2.16)$$

In Eq. (2.16), the volume of integration V is all of three-dimensional space. However, as discussed in Sec. 1.4.1, only scatterers within a single resolution cell volume ΔV contribute significantly to the radar receiver output at any given instant. Thus, a more appropriate form of the generalized radar range equation is

$$P_r = \frac{P_t \lambda^2}{(4\pi)^3 L_s} \int_{\Delta V(R, \theta, \phi)} \frac{P^2(\theta, \phi)}{R^4 L_a(R)} d\sigma(R, \theta, \phi) \quad (2.17)$$

where $\Delta V(R_0, \theta_0, \phi_0)$ is the volume of the resolution cell at nominal coordinates (R_0, θ_0, ϕ_0) .

By integrating power, it is being assumed that the backscatter from each volume element adds *noncoherently* rather than *coherently*. This means that the power of the composite electromagnetic wave formed from the backscatter of two or more scattering centers is the sum of the individual powers, as opposed to the voltage (electric field amplitude) being the sum of the individual amplitudes, in which case the power would be the square of the voltage sum. Noncoherent addition occurs when the phases of the individual contributors are random and

uncorrelated with one another, as opposed to the coherent case when they are in phase.

The general result of Eq. (2.17) is more useful if evaluated for the special cases of point, volume, and area scatterers. Beginning with the point scatterer, the differential RCS in the resolution cell volume is represented by a Dirac impulse function of weight σ :

$$d\sigma(R, \theta, \phi) = \sigma \delta_D(R - R_0, \theta - \theta_0, \phi - \phi_0) dV \text{ (point scatterer)} \quad (2.18)$$

Using Eq. (2.18) in Eq. (2.17) gives the range equation for a point target

$$P_r = \frac{P_t P^2(\theta_0, \phi_0) \lambda^2 \sigma}{(4\pi)^3 R_0^4 L_s L_a(R_0)} \quad (2.19)$$

If the point scatterer is located on the antenna boresight $\theta_0 = \phi_0 = 0$, $P(\theta_0, \phi_0) = G$ and Eq. (2.19) is identical to Eq. (2.11).

Next consider the *volume scattering* case where the RCS seen by the radar is presumed to be due to a distribution of scatterers evenly distributed throughout the volume, rather than associated with a single point. In this case, σ is expressed in terms of RCS per cubic meter, or *volume reflectivity*, denoted as η . The units of reflectivity are $\text{m}^2/\text{m}^3 = \text{m}^{-1}$. The RCS of a differential volume element dV is just

$$d\sigma = \eta dV = \eta R^2 dR d\Omega \text{ (volume scatterer)} \quad (2.20)$$

where $d\Omega$ is a differential solid angle element. The range equation becomes

$$P_r = \frac{P_t \lambda^2 \eta}{(4\pi)^3 L_s} \int_{\Delta V(R, \theta, \phi)} \frac{P^2(\theta, \phi)}{R^2 L_a(R)} dR d\Omega \quad (2.21)$$

Consider integration over the range coordinate first. If it is assumed that atmospheric loss is very slowly varying over the extent of a range resolution cell, then $L_a(R)$ can be replaced by $L_a(R_0)$ and removed from the integral. The integral over range that remains is

$$\int_{R_0 - \frac{\Delta R}{2}}^{R_0 + \frac{\Delta R}{2}} \left(\frac{dR}{R^2} \right) = \frac{\Delta R}{R_0^2 - (\Delta R/2)^2} \approx \frac{\Delta R}{R_0^2} \quad (2.22)$$

provided the range resolution is small compared to the absolute range, which is usually the case. Using Eq. (2.22) in Eq. (2.21) gives

$$P_r = \frac{P_t \lambda^2 \eta \Delta R}{(4\pi)^3 R_0^2 L_s L_a(R_0)} \int_{\Delta \Omega} P^2(\theta, \phi) d\Omega \quad (2.23)$$

Integration over the angular coordinates requires knowledge of the antenna pattern. The main lobe of many antennas can be reasonably well approximated

by a Gaussian function (Sauvageot, 1992). It can be shown that a good approximation to the integral in Eq. (2.23) over the cross-range variables for the Gaussian case is (Probert-Jones, 1962)

$$\iint P^2(\theta, \phi) d\theta d\phi \approx \frac{\pi \theta_3 \phi_3}{8 \ln 2} G^2 = 0.57 \theta_3 \phi_3 G^2 \quad (2.24)$$

where θ_3 and ϕ_3 are the 3-dB beamwidths in azimuth and elevation. For first-order calculations, the even simpler assumption is frequently made that the antenna power pattern $P(\theta, \phi)$ is a constant equal to the gain G over the 3-dB beamwidths and zero elsewhere, so that the integral reduces to $G^2 \theta_3 \phi_3$, a value 2.5 dB higher than that of Eq. (2.24). Using this simpler approximation, Eq. (2.23) reduces to the range equation for volume scatterers:

$$P_r = \frac{P_t G^2 \lambda^2 \eta \Delta R \theta_3 \phi_3}{(4\pi)^3 R_0^2 L_s L_a(R_0)} \text{ (volume scatterers)} \quad (2.25)$$

Unlike the point scatterer case described by Eq. (2.11) or (2.19), the received power in the volume scattering case of Eq. (2.25) decreases only as R^2 instead of R^4 . The reason is that the size of the radar resolution cell, which determines the extent of the scatterers contributing to the received power at any one instant, increases as R^2 due to the spreading of the antenna beam in angle at longer ranges.

Finally, the *area scattering* case will be considered. This model is used for the RCS of electromagnetic scatter from the ground, forest, ocean, and other surfaces that have a large area relative to the antenna beam main lobe. The area scattering case must further be divided into two subcases depending on whether the range extent of the scatterers contributing to the echo is limited by the antenna elevation beamwidth or by the range resolution.

First assume that the scattering surface is represented by a flat plane[†] and consider the extent of the main lobe on the surface. The cross-range extent is simply $R_0 \theta_3$, where R_0 is the nominal range to the center of the illuminated area. To estimate the down-range extent, consider Fig. 2.1 that shows the bore-sight vector intersecting the scattering plane at a *grazing angle* of δ radians. The extent of the beam “footprint” in the down-range dimension is therefore $R_0 \phi_3 / \sin \delta$ meters.

Now suppose a pulse of range resolution ΔR is transmitted as shown in Fig. 2.2. Regardless of the antenna footprint, the range extent of scatterers within the resolution cell, and therefore emitting backscattered energy at any instant, is $\Delta R / \cos \delta$ meters.

Scatterers will not contribute to the received signal unless they are both illuminated (so that there is some backscatter) and within the main lobe of the antenna (so that their backscatter is not excessively attenuated). Consequently,

[†]This ignores earth curvature effects that are significant in very long range or spaceborne radars. See the books by Nathanson (1991) or Skolnik (2001) for additional details.

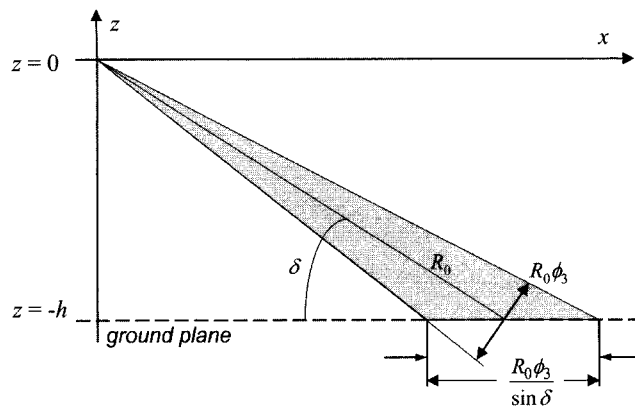


Figure 2.1 Projection of elevation beamwidth onto a horizontal plane at a slant range R_0 and grazing angle δ .

the effective down-range extent of the resolution cell is the lesser of the range resolution and the elevation beamwidth as each is projected onto the scattering surface. Depending on the relative values of range, range resolution, and grazing angle, either could be the limiting factor. If the range resolution limits the effective extent, the resolution cell is said to be *pulse limited*; if the main lobe extent is the limiting factor, it is said to be *beam limited*. These two cases are shown in Fig. 2.3.

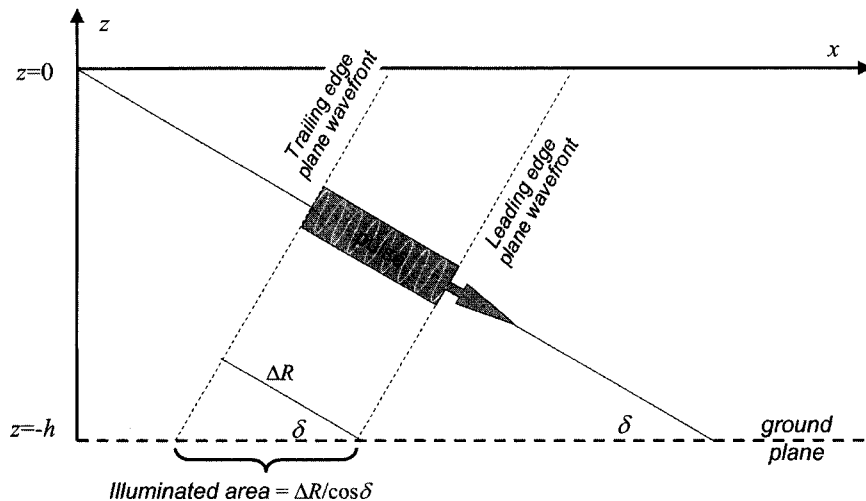


Figure 2.2 Projection of range resolution onto a horizontal plane at a slant range R_0 and grazing angle δ .

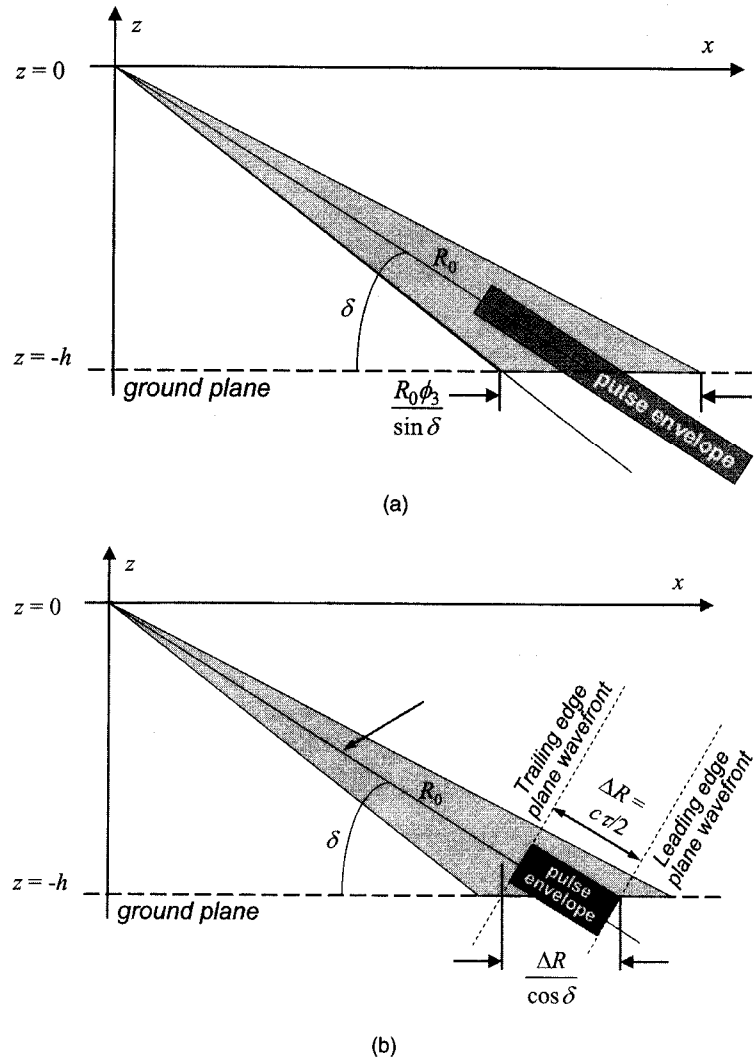


Figure 2.3 Relative geometry of antenna footprint and pulse envelope.
(a) Beam-limited case. (b) Pulse-limited case.

The boundary between the two cases is

$$\begin{aligned}
 \text{Beam-limited: } & \frac{\Delta R}{R_0} \tan \delta > \phi_3 \\
 \text{Pulse-limited: } & \frac{\Delta R}{R_0} \tan \delta < \phi_3
 \end{aligned} \tag{2.26}$$

In area scattering, all of the differential RCS is due to backscatter from a surface at a particular range within the resolution cell, say R_0 ; the remainder

of the cell contributes no scattering. In this case, the differential volume RCS of Eq. (2.20) is proportional to the differential area of the scattering surface and can be represented as

$$d\sigma = \delta_D(R - R_0)\sigma^0 dA \quad (2.27)$$

where σ^0 (called “sigma-nought”) is the RCS in m^2/m^2 and is therefore dimensionless. The generalized range equation becomes

$$\begin{aligned} P_r &= \frac{P_t \lambda^2 \sigma^0}{(4\pi)^3 L_s} \int_{\Delta A(R_0, \theta_0, \phi_0)} \frac{P^2(\theta, \phi)}{R^4 L_a(R)} \delta(R - R_0) dA \\ &= \frac{P_t \lambda^2 \sigma^0}{(4\pi)^3 R_0^4 L_s L_a(R_0)} \int_{\Delta A(R_0, \theta, \phi)} P^2(\theta, \phi) dA \end{aligned} \quad (2.28)$$

where $\Delta A(R_0, \theta, \phi)$ is the illuminated area at range R_0 .

If the illuminated area is beam-limited, applying the geometry of Fig. 2.3a to the differential scattering element at range R_0 shows that the area contributing to the backscatter at one instant is $R^2 \phi_3 \theta_3 / \sin \delta$. Thus, a differential area contributing to the received power is of the form

$$dA = R_0 d\theta \frac{R_0}{\sin \delta} d\phi = \frac{R_0^2}{\sin \delta} d\theta d\phi \quad (\text{beam-limited case}) \quad (2.29)$$

Applying this to Eq. (2.28) and again using the constant-gain approximation to the antenna 3-dB beamwidth gives the beam-limited range equation for area scatterers:

$$P_r = \frac{P_t G^2 \lambda^2 \phi_3 \theta_3 \sigma^0}{(4\pi)^3 R_0^2 L_s L_a(R_0) \sin \delta} \quad (\text{area scatterers, beam-limited case}) \quad (2.30)$$

If the illuminated area is pulse limited, the geometry of Fig. 2.3b shows that the area contributing to the backscatter at one instant is $R \theta_3 \Delta R / \cos \delta$. The differential contribution is thus

$$dA = R_0 d\theta \frac{\Delta R}{\cos \delta} d\phi = \frac{R_0 \Delta R}{\cos \delta} d\theta d\phi \quad (\text{pulse-limited case}) \quad (2.31)$$

The first-order approximation of constant gain over the main lobe can be used again, though the integral over ϕ is now limited to the range that covers the extent of the pulse on the ground. Equation (2.28) becomes

$$P_r = \frac{P_t G^2 \lambda^2 \sigma^0 \Delta R \theta_3}{(4\pi)^3 R_0^3 L_s L_a(R_0) \cos \delta} \quad (\text{area scatterers, pulse-limited case}) \quad (2.32)$$

Note that power varies as R^{-2} in the beam-limited case because, as with the volume scattering, the resolution cell size grows in both cross-range and down-range extent with increasing range. In the pulse-limited case, power varies as R^{-3} because the resolution cell extent increases in only the cross-range dimension with increasing range.

2.2.3 Radar cross section

Section 2.2.1 introduced the radar cross section to heuristically account for the amount of power reradiated by the target back toward the radar transmitter. To restate the concept, assume that the incident power density at the target is Q_t and the backscattered power density at the transmitter is Q_b . If that backscattered power density resulted from isotropic radiation from the target, it would have to satisfy

$$Q_b = \frac{P_b}{4\pi R^2} \quad (2.33)$$

for some total backscattered power P_b . RCS is the *fictional* area over which the transmitted power density Q_t must be intercepted to collect a total power P_b that would account for the received power density, that is, σ must satisfy

$$P_b = \sigma Q_t \quad (2.34)$$

Combining Eqs. (2.33) and (2.34) gives

$$\sigma = 4\pi R^2 \frac{Q_b}{Q_t} \quad (2.35)$$

This definition is usually written in terms of electric field amplitude. Also, in order to make the definition dependent only on the target characteristics, range is eliminated by taking the limit as R tends to infinity. Thus, the formal definition of radar cross section becomes (Knott, Shaeffer, and Tuley, 1985)

$$\sigma = 4\pi \lim_{R \rightarrow \infty} \left[R^2 \frac{|\mathbf{E}^b|^2}{|\mathbf{E}^t|^2} \right] \quad (2.36)$$

where $|\mathbf{E}^b|^2$ and $|\mathbf{E}^t|^2$ are the backscattered and transmitted electric field squared magnitudes, respectively.

The RCS just defined is a single real scalar number. Implicit in the definition is the use of a single polarization of the transmitted wave and a single receiver polarization, usually the same as the transmitted polarization. However, the polarization state of a transverse electromagnetic plane wave is a two-dimensional vector, and therefore two orthogonal polarization basis vectors are required to fully describe the wave. The most common basis choices are linear (horizontal and vertical polarizations) and circular (left and right rotating polarizations). Furthermore, a general target will modify the polarization of an incident wave, so that the energy backscattered from, say, the vertical component of the incident wave may have both vertical and horizontal components. To account fully for polarization effects, RCS must be generalized to the *polarization scattering matrix* (PSM) \mathbf{S} , which relates the complex amplitudes of the

incident and backscattered fields. For a radar using a linear polarization basis, e.g., this relation is (Knott, Shaeffer, and Tuley, 1985; Mott, 1986; Holm, 1987)

$$\begin{bmatrix} \mathbf{E}_H^b \\ \mathbf{E}_V^b \end{bmatrix} = \begin{bmatrix} S_{HH} & S_{HV} \\ S_{VH} & S_{VV} \end{bmatrix} \begin{bmatrix} \mathbf{E}_H^t \\ \mathbf{E}_V^t \end{bmatrix}$$

$$= \mathbf{S} \begin{bmatrix} \mathbf{E}_H^t \\ \mathbf{E}_V^t \end{bmatrix} \quad (2.37)$$

Instead of a single real number, the target backscattering characteristics are now described by four complex numbers. If the radar transmitted and received, say, only the vertical component, then the RCS σ would be related to \mathbf{S} by

$$\sigma = |S_{VV}|^2 \quad (2.38)$$

Radars can be designed to measure the full PSM. Other designs measure the magnitudes of the elements of the PSM, but not the phases, or the magnitudes of two of the PSM elements. These *polarimetric* measurements can be used for a variety of target analysis purposes. However, a discussion of polarimetric techniques is beyond the scope of this book. Henceforth, it will be assumed that only a single fixed polarization is transmitted and a single fixed polarization received, and consequently that RCS is described by a scalar, rather than matrix, function. The reader is referred to the works by Holm (1987) and Mott (1986) for discussions of polarimetric radars and polarimetric signal processing.

Typical values of RCS for targets of interest range from 0.01 m^2 (-20 dB with respect to 1 m^2 , or -20 dBsm) to hundreds of square meters ($\geq +20 \text{ dBsm}$). Both larger and smaller values are also observed. Table 2.1 lists representative RCS values for various types of targets.

TABLE 2.1 Typical RCS Values at Microwave Frequencies

Target	RCS, m^2	RCS, dBsm
Conventional unmanned winged missile	0.5	-3
Small single-engine aircraft	1	0
Small fighter aircraft or 4-passenger jet	2	3
Large fighter aircraft	6	8
Medium bomber or jet airliner	20	13
Large bomber or jet airliner	40	16
Jumbo jet	100	20
Small open boat	0.02	-17
Small pleasure boat	2	3
Cabin cruiser	10	10
Large ship at zero grazing angle	10,000+	40+
Pickup truck	200	23
Automobile	100	20
Bicycle	2	3
Man	1	0
Bird	0.01	-20
Insect	0.00001	-50

SOURCE: After Skolnik (2001).

2.2.4 Radar cross section for meteorological targets

The field of radar meteorology expresses the reflectivity of weather targets such as rain or snow in terms of a normalized factor called the *reflectivity* (here called the *volume reflectivity*) and usually represented with the symbol Z (Sauvageot, 1992; Doviak and Zrnic, 1993). Weather targets are an example of volume clutter. The actual observed echo is the composite backscatter of many raindrops, suspended water particles, or snowflakes in the radar's resolution cell.

Suppose the RCS of the i th individual scatterer is σ_i . Then the total RCS of a volume V containing N such scatterers is $\sum \sigma_i$ and the volume reflectivity is

$$\eta = \frac{1}{\Delta V} \sum_{i=1}^N \sigma_i \quad (2.39)$$

Water droplets are often modeled as small conducting spheres. When the ratio of the sphere radius a to the radar wavelength λ is small, specifically $2\pi a/\lambda \ll 1$, the radar cross section associated with the i th scatterer can be expressed as

$$\sigma_i = \frac{\pi^5 |K|^2 D_i^6}{\lambda^4} \quad (2.40)$$

where D_i is the drop diameter, usually given in millimeters and

$$K = \frac{m^2 - 1}{m^2 + 1} \quad (2.41)$$

and m is the complex index of refraction. The index of refraction is a function of both the temperature and wavelength. However, for wavelengths between 3 and 10 cm (radar frequencies between X band (10 GHz) and C band (3 GHz)) and temperatures between 0°C and 20°C, the value of $|K|^2$ is approximately a relatively constant 0.93 for scatterers composed of water and 0.197 for ice. Substituting Eq. (2.40) in Eq. (2.39) gives

$$\eta = \frac{1}{\Delta V} \sum_{i=1}^N \frac{\pi^5 |K|^2 D_i^6}{\lambda^4} = \frac{\pi^5 |K|^2}{\lambda^4} \frac{1}{\Delta V} \sum_{i=1}^N D_i^6 \quad (2.42)$$

Now define the quantity

$$Z \equiv \frac{1}{\Delta V} \sum_{i=1}^N D_i^6 \quad (2.43)$$

Z is called the *volume reflectivity* and is usually expressed in units of mm^6/m^3 . Due to the large range of values observed for Z , it is commonly expressed on a decibel scale and denoted as dBz . Using this definition in Eq. (2.42) gives the following expression for the observed RCS

$$\eta = \frac{\pi^5 |K|^2}{\lambda^4} Z \quad (2.44)$$

TABLE 2.2 Correspondence between dBz Reflectivity and Rain Rate

Level	Rain fall rate (mm/hr)	Reflectivity dBz	Category
1	0.49 to 2.7	18 to <30	Light mist
2	2.7 to 13.3	30 to <41	Moderate
3	13.3 to 27.3	41 to <46	Heavy
4	27.3 to 48.6	46 to <50	Very Heavy
5	48.6 to 133.2	50 to <57	Intense
6	133.2 and greater	57 and above	Extreme

Thus, given a measured echo power, the radar range equation can be used to estimate η , and then Eq. (2.44) can be used to convert η to Z .

Because it is related only to the volume density and size of scatterers, meteorologists prefer to express radar echo strength in terms of the reflectivity Z rather than the RCS η . The value of Z can then be related to the amount of water in the air or the precipitation rate. A number of models are used to relate the observed values of Z to rain rates. These models depend on the type of precipitation, e.g., snow versus thunderstorm rain versus “orographic”[†] rain. The most common model is that of Table 2.2, which shows the six-level equivalence between observed Z values (in dBz) and rainfall rates used in the U.S. NEXRAD national weather radar system. Very similar scales are used in the commercial “Doppler weather radar” systems familiar to every watcher of television weather forecasts.

It is important to note that the dBz values in Table 2.2 are 10 times the base 10 logarithm of Z in mm^6/m^3 . When Z is given in $\text{m}^6/\text{m}^3 = \text{m}^3$, it must be multiplied by 10^{18} to convert it to units of mm^6/m^3 before converting to a decibel scale and using Table 2.2.

2.2.5 Statistical description of radar cross section

The radar cross section of real targets cannot be effectively modeled as a simple constant. In general, RCS is a complex function of aspect angle, frequency, and polarization, even for relatively simple scatterers. For example, the conducting trihedral corner reflector of Fig. 2.4 is often used as a calibration target in field measurements. Its RCS when viewed along its axis of symmetry (looking “into the corner”) can be determined theoretically; it is (Knott, Shaeffer, and Tuley, 1985)

$$\sigma = \frac{12\pi a^4}{\lambda^2} \quad (2.45)$$

Thus the RCS increases with increasing frequency. On the other hand, at least one frequency- and aspect-independent scatterer exists. The RCS of a conducting sphere of radius a is a constant πa^2 , provided $a \gg \lambda$. It is independent of aspect angle because of the spherical symmetry.

[†]A form of rain that occurs when moist air is lifted over an obstacle such as a mountain range, cooling as it rises and condensing into rainfall.

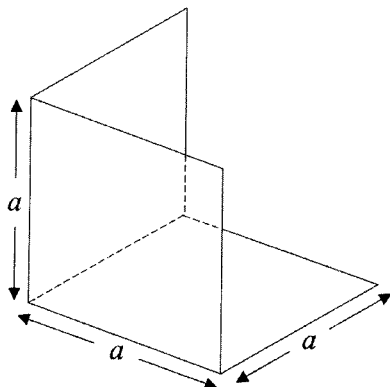


Figure 2.4 Square trihedral corner reflector.

A simple example of frequency and aspect dependence is the two-scatterer “dumbbell” target of Fig. 2.5. If the nominal range R is much greater than the separation D , the range to the two scatterers is approximately

$$R_{1,2}(\theta) \approx R \pm \frac{D}{2} \sin \theta \quad (2.46)$$

If the signal $a e^{j2\pi F t}$ is transmitted, the echo from each scatterer will be proportional to $a e^{j2\pi F(t-2R_{1,2}(\theta)/c)}$. The voltage $\bar{y}(t)$ of the composite echo is therefore proportional to

$$\begin{aligned} \bar{y}(t) &= a e^{j2\pi F(t-2R_1(\theta)/c)} + a e^{j2\pi F(t-2R_2(\theta)/c)} \\ &= a e^{j2\pi F(t-2R/c)} [e^{-j\pi FD \sin \theta / c} + e^{+j\pi FD \sin \theta / c}] \\ &= 2a e^{j2\pi F(t-2R/c)} \cos(\pi FD \sin \theta / c) \end{aligned} \quad (2.47)$$

RCS is proportional to the power of the composite echo. Taking the squared magnitude of Eq. (2.47) and simplifying leads to the result

$$\sigma = 4a^2 |\cos(\pi FD \sin \theta / c)|^2 = 4a^2 |\cos(\pi D \sin \theta / \lambda)|^2 \quad (2.48)$$

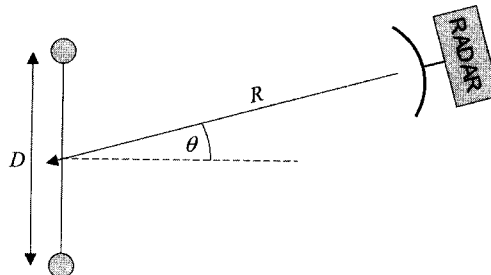


Figure 2.5 Geometry for determining relative RCS of a “dumbbell” target.

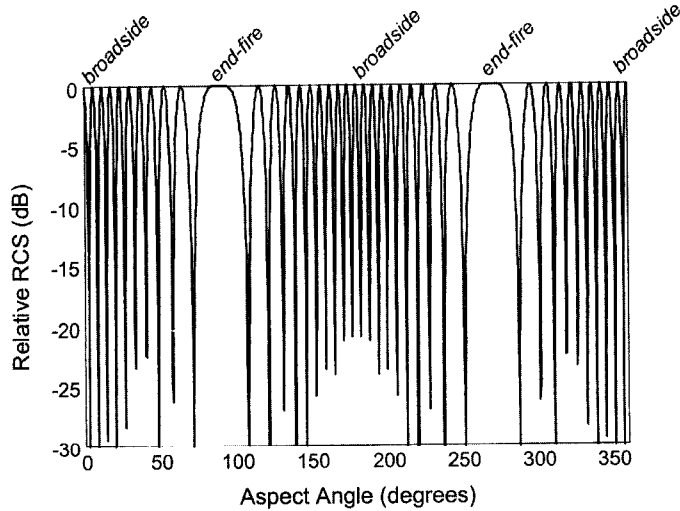


Figure 2.6 Relative radar cross section of the “dumbbell” target of Fig. 2.5 when $D = 10\lambda$ and $R = 10,000D$.

Equation (2.48) shows that the RCS is a periodic function of both radar frequency and aspect angle. The larger the scatterer separation in terms of wavelengths, the more rapidly the RCS varies with angle or frequency. An exact calculation of the variation in RCS of the dumbbell target is plotted in Fig. 2.6 for the case $D = 10\lambda$ and $R = 10,000D$. The plot has been normalized so that the maximum value corresponds to 0 dB. Notice the multilobed structure as the varying path lengths traversed by the echoes from the two scatterers cause their echoes to shift between constructive and destructive interference. Also note that the maxima at aspect angles of 90° and 270° (the two “end fire” cases) are the broadest, while the maxima at the two “broadside” cases of 0° and 180° are the narrowest. Figure 2.7 plots the same data in a more traditional polar format.

The relative RCS of a target with multiple scatterers can be computed using a generalization of Eq. (2.47). Suppose there are N scatterers, each with its own RCS σ_i , located at ranges $R_i(\theta)$ from the radar. Note that the ranges R_i vary with aspect angle θ . The complex voltage of the echo will be, to within a proportionality constant

$$\begin{aligned}
 \bar{y}(t) &= \sum_{i=1}^N \sqrt{\sigma_i} e^{j2\pi F(t-2R_i(\theta)/c)} \\
 &= e^{j2\pi F t} \sum_{i=1}^N \sqrt{\sigma_i} e^{-j4\pi F R_i(\theta)/c} \\
 &= e^{j2\pi F t} \sum_{i=1}^N \sqrt{\sigma_i} e^{-j4\pi R_i(\theta)/\lambda}
 \end{aligned} \tag{2.49}$$

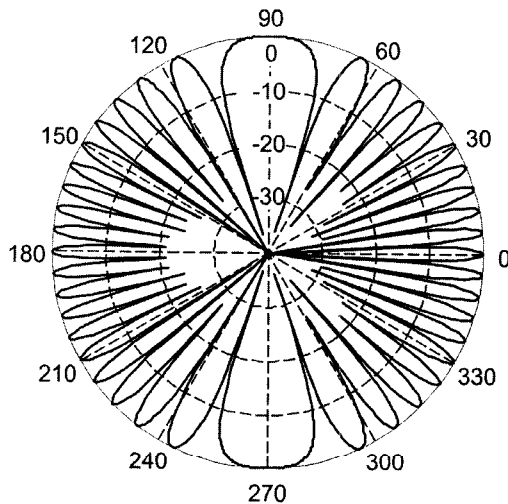


Figure 2.7 Polar plot of the data of Fig. 2.6.

The RCS σ is proportional to $|\bar{y}|^2$. Define

$$\zeta \equiv |\bar{y}| = \left| \sum_{i=1}^N \sqrt{\sigma_i} e^{-j4\pi R_i(\theta)/\lambda} \right| \quad (2.50)$$

and

$$\sigma = \zeta^2 = \left| \sum_{i=1}^N \sqrt{\sigma_i} e^{-j4\pi R_i(\theta)/\lambda} \right|^2 \quad (2.51)$$

RCS variations like those of Fig. 2.6 become very complicated for complex targets having many scatterers of varying individual RCS. Figure 2.8 shows a “target” consisting of 50 point scatterers randomly distributed within a rectangle 5 m wide and 10 m long. The RCS of each individual point scatterer is a

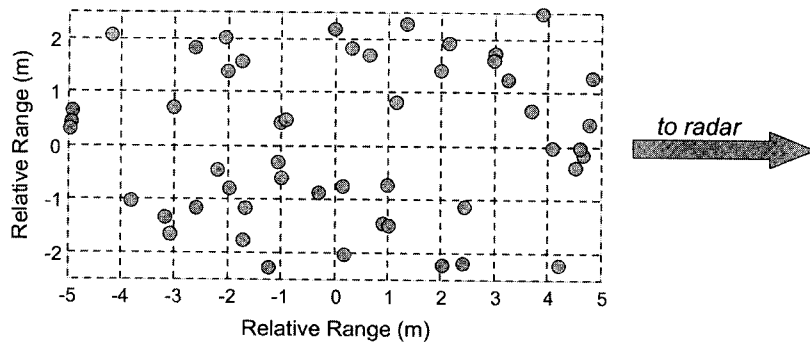


Figure 2.8 Random distribution of 50 scatterers used to obtain Fig. 2.9. (See text for additional details.)

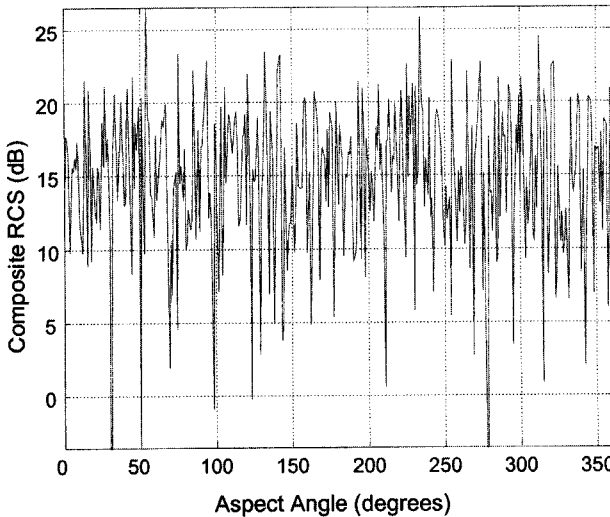


Figure 2.9 Relative RCS of the complex target of Fig. 2.8 at a range of 10 km and radar frequency of 10 GHz.

constant, $\sigma_i = 1.0$. Figure 2.9 shows the relative RCS, computed at 0.2° increments using Eq. (2.51), which results when this target is viewed 10 km from its center at a frequency of 10 GHz. The dynamic range is similar to that of the simple dumbbell target, but the lobing structure is much more complicated.

The complicated behavior observed for even moderately complex targets leads us to use a statistical description for radar cross section (Levanon, 1988; Nathanson, 1991; Skolnik, 2001). This means that the RCS σ of the scatterers within a single resolution cell is considered to be a random variable with a specified *probability density function* (pdf). The radar range equation is used to estimate the mean RCS, and one of a variety of pdfs are used to describe the statistical behavior of the RCS.

Consider first a target consisting of a large number of individual scatterers (similar to that of Fig. 2.8), each with its own individual but fixed RCS and randomly distributed in space. It can be assumed that the phase of the echoes from the various scatterers is a random variable distributed uniformly on $(0, 2\pi]$. Under these circumstances, the central limit theorem guarantees that the real and imaginary parts of the composite echo can each be assumed to be independent, zero mean Gaussian random variables with the same variance, say α^2 (Papoulis, 1984; Beckmann and Spizzichino, 1963). In this case, the squared-magnitude σ has an exponential pdf (Papoulis, 1984):

$$p_\sigma(\sigma) = \begin{cases} \frac{1}{\bar{\sigma}} \exp\left[\frac{-\sigma}{\bar{\sigma}}\right] & \sigma \geq 0 \\ 0 & \sigma < 0 \end{cases} \quad (2.52)$$

where $\bar{\sigma} = 2\alpha^2$ is the mean value of the RCS σ . The voltage or magnitude ζ has a Rayleigh pdf

$$p_{\zeta}(\zeta) = \begin{cases} \frac{2\zeta}{\bar{\sigma}} \exp\left[-\frac{\zeta^2}{\bar{\sigma}}\right] & \zeta \geq 0 \\ 0 & \zeta < 0 \end{cases} \quad (2.53)$$

While the Rayleigh/exponential model is only strictly accurate in the limit of a very large number of scatterers, in practice it can be a good model for a target having as few as 10 or 20 significant scatterers. Figure 2.10 compares a histogram of the RCS values from Fig. 2.9 to an exponential curve of the form of Eq. (2.52) having the same mean $\bar{\sigma}$. Even though only 50 scatterers are used, the fit of the total RCS histogram to the Rayleigh/exponential distribution is quite good. This same effect is observed when the randomly distributed scatterers also have random individual cross sections drawn from the same Gaussian distribution, a somewhat more general and plausible situation than the fixed-RCS case.

Many radar targets are not well modeled as an ensemble of equal-strength scatterers, so many other pdfs have been advocated and used. Table 2.3 summarizes several of the more common RCS models. The mean value $\bar{\sigma}$ of RCS is given for each case in which the pdf is not written explicitly in terms of $\bar{\sigma}$. The variance $\text{var}(\sigma)$ is given for each case. The naming terminology can be confusing, because in some cases the name traditionally applied to the distribution of RCS σ is actually that of the density function of the corresponding amplitude ζ . For example, the exponential RCS distribution of Eq. (2.52) is frequently referred to as the Rayleigh model.

The shape of the pdf of RCS directly affects detection performance, as is seen in Chap. 6. Figure 2.11a compares the Rayleigh/exponential, fourth-degree chi-square, Rice, Weibull, and log-normal density functions when all have an

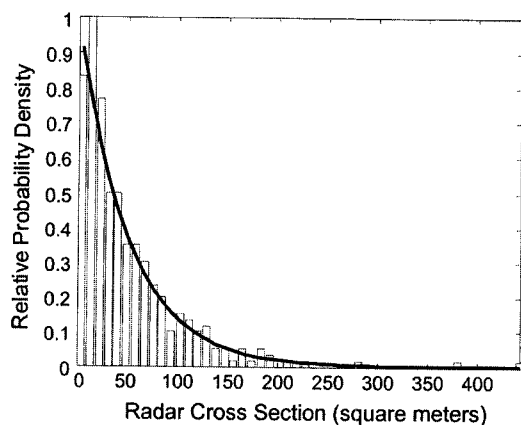


Figure 2.10 Histogram of RCS data of Fig. 2.9 and exponential pdf with the same mean.

TABLE 2.3 Common Statistical Models for Radar Cross Section

Model name	pdf for RCS σ	Comment
Nonfluctuating, Marcum, Swerling 0, or Swerling 5	$p_\sigma(\sigma) = \delta_D(\sigma - \bar{\sigma})$ $\text{var}(\sigma) = 0$	Constant echo power, e.g., calibration sphere or perfectly stationary reflector with no radar or target motion.
Rayleigh/exponential, chi-square of degree 2	$p_\sigma(\sigma) = \frac{1}{\bar{\sigma}} \exp\left[\frac{-\sigma}{\bar{\sigma}}\right]$ $\text{var}(\sigma) = \bar{\sigma}^2$	Many scatterers, randomly distributed, none dominant. Used in Swerling case 1 and 2 models.
Chi-square of degree 4	$p_\sigma(\sigma) = \frac{4\sigma}{\bar{\sigma}^2} \exp\left[\frac{-2\sigma}{\bar{\sigma}}\right]$ $\text{var}(\sigma) = \bar{\sigma}^2/2$	Approximation to case of many small scatterers + one dominant, with RCS of dominant equal to $1 + \sqrt{2}$ times the sum of RCS of others. Used in Swerling case 3 and 4 models.
Chi-square of degree $2m$, Weinstock	$p_\sigma(\sigma) = \frac{m}{\Gamma(m)\bar{\sigma}} \left[\frac{m\sigma}{\bar{\sigma}}\right]^{m-1} \exp\left[\frac{-m\sigma}{\bar{\sigma}}\right]$ $\text{var}(\sigma) = \bar{\sigma}^2/m$	Generalization of the two preceding cases. Weinstock cases correspond to $0.6 \leq 2m \leq 4$. Higher degrees correspond to presence of a more dominant single scatterer.
Rice or Rician, noncentral chi-square of degree 2	$p_\sigma(\sigma) = \frac{1}{\bar{\sigma}}(1+a^2) \exp\left[-a^2 - \frac{\sigma}{\bar{\sigma}}(1+a^2)\right]$ $\times I_0\left[2a\sqrt{(1+a^2)(\sigma/\bar{\sigma})}\right]$ $\text{var}(\sigma) = \frac{(1+2a^2)}{(1+a^2)^2} \bar{\sigma}^2$	Exact solution for one dominant scatterer plus many small ones. Ratio of dominant RCS to sum of small RCS is a^2 .
Weibull	$p_\sigma(\sigma) = CB\sigma^{C-1} \exp[-B\sigma^C]$ $\bar{\sigma} = \Gamma(1+1/C)B^{-1/C}$ $\text{var}(\sigma) = B^{-2/C}[\Gamma(1+2/C) - \Gamma^2(1+1/C)]$	Empirical fit to many measured target and clutter distributions. Can have longer "tail" than previous cases.
Log-normal	$p_\sigma(\sigma) = \frac{1}{\sqrt{2\pi}s\sigma} \exp\left[-\ln^2(\sigma/\sigma_m)/2s^2\right]$ $\bar{\sigma} = \sigma_m \exp(s^2/2)$ $\text{var}(\sigma) = \sigma_m^2 \exp(s^2)[\exp(s^2) - 1]$	Empirical fit to many measured target and clutter distributions. "Tail" is longest of previous cases. σ_m is the median value of σ .

RCS variance of 0.5. The exponential distribution then necessarily has a mean of $\sqrt{0.5}$. The fourth-degree chi-square necessarily has a mean of 1.0, and the parameters of the remaining density functions have been chosen to give them a mean of 1.0 as well. Figure 2.11b repeats the same data on a semilogarithmic scale so that the behavior of the pdf "tails" is more evident. Note that the Weibull and Rice distributions are very similar. The chi-square is also similar, but has a somewhat less extensive tail to the distribution. The log-normal has both the narrowest peak and the longest tail of any of the distributions shown. Unlike all of the others, the exponential does not peak near the mean RCS. Each of the others does have a distinct peak, making them suitable for distributions with one or a few dominant scatterers.

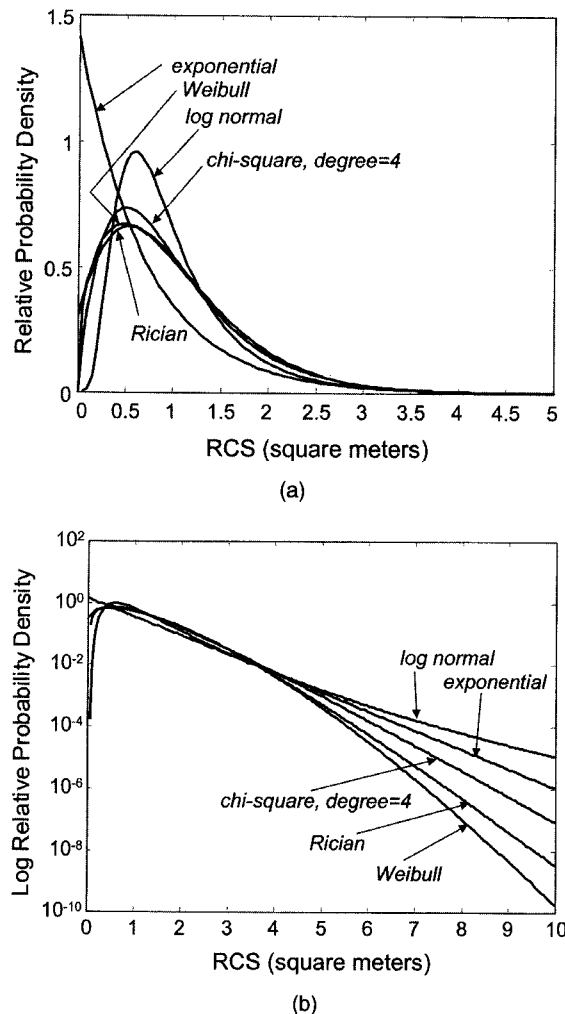


Figure 2.11 Comparison of five models for the probability density function of radar cross section. (See text for additional details.) (a) Linear scale. (b) Log scale.

One fundamental difference among the various RCS models of Table 2.3 is whether the probability density function has one or two free parameters. The nonfluctuating, Rayleigh/exponential, and all chi-square (once the order is stated) are all *one-parameter distributions*. The one parameter in the form given earlier is the mean RCS, $\bar{\sigma}$. The Rice, Weibull, and log-normal are *two-parameter distributions*. The parameters are $\bar{\sigma}$ and a^2 for the Rice, B and C for the Weibull, and σ_m and s for the log-normal in the forms given. For a one-parameter distribution, estimating the mean also provides an estimate of the variance. For the two-parameter case, separate estimates of mean and variance

must be computed. This distinction is important in the design of automatic detection algorithms in Chap. 7.

Most radar analysis and measurement programs emphasize RCS measurements, which are proportional to received power. Sometimes ζ , the corresponding voltage, is of interest, particularly for use in simulations where Eq. (2.49) is used explicitly to model the composite echo from a multiple scatterer target. The probability density function for the voltage is required in order to properly model the probabilistic variations of the complex sum. The pdf of $|\zeta|$ is easily derived from the pdf of σ using basic results of random variables (Papoulis, 1984). Because RCS is nonnegative, the transformation[†]

$$\zeta = \sqrt{\sigma} \quad (2.54)$$

from RCS to voltage has only one real solution for σ , namely $\sigma = \zeta^2$. It then follows that the pdf of ζ is given by

$$\begin{aligned} p_\zeta(\zeta) &= \frac{p_\sigma(\zeta^2)}{d\zeta/d\sigma} \\ &= 2\zeta p_\sigma(\zeta^2) \end{aligned} \quad (2.55)$$

Equation (2.55) can be used to write the voltage pdfs by inspection from Table 2.3. The results, given in Table 2.4, are expressed in terms of the parameters of the corresponding RCS distribution from Table 2.3. Note that the nonfluctuating, Weibull, and log-normal RCS distributions all result in distributions of the same type (but with one or more parameters changed) for the voltage. Also note that the voltage in the Rayleigh/exponential case is Rayleigh distributed, explaining the name.

As has been seen, the RCS of a complex target varies with both transmitted frequency and aspect angle. Another important characteristic of a target's signature is the *correlation "length"* in time, frequency, and angle. This is the change in time, frequency, or angle required to cause the echo amplitude to decorrelate to a specified degree. If a rigid target such as a building is illuminated with a series of identical radar pulses and there is no motion between the radar and target, one expects the same received complex voltage y from each pulse (ignoring receiver noise). If motion between the two is allowed, however, the relative path length between the radar and the various scatterers comprising the target will change, causing the composite echo amplitude to fluctuate. Thus, for rigid targets, decorrelation of the RCS is induced by changes in range and aspect angle. On the other hand, if natural clutter such as the ocean surface or a stand of trees is illuminated, the signature will decorrelate even if the radar and target do not move relative to one another. In this case the decorrelation

[†]Because the power P of a real sinusoid is related to its amplitude A according to $P = A^2/2$ instead of just $P = A^2$, some authors (e.g., Levanon (1988)) present a slightly different form for the voltage distributions.

TABLE 2.4 Voltage Distributions Corresponding to Common Statistical Models of Radar Cross Section

RCS model name	pdf for voltage ζ	Comment
Nonfluctuating, Marcum, Swerling 0, or Swerling 5	$p_\zeta(\zeta) = \delta_D(\zeta - \sqrt{\bar{\sigma}})$ $\bar{\zeta} = \sqrt{\bar{\sigma}}, \quad \text{var}(\zeta) = 0$	Also nonfluctuating model.
Rayleigh/exponential, chi-square of degree 2	$p_\zeta(\zeta) = \frac{2\zeta}{\bar{\sigma}} \exp\left[\frac{-\zeta^2}{\bar{\sigma}}\right]$ $\bar{\zeta} = \frac{1}{2}\sqrt{\pi\bar{\sigma}}, \quad \text{var}(\zeta) = \bar{\sigma}(1 - \pi/4)$	Rayleigh distribution. RCS has exponential distribution.
Chi-square of degree 4	$p_\zeta(\zeta) = \frac{8\zeta^3}{\bar{\sigma}^2} \exp\left[\frac{-2\zeta^2}{\bar{\sigma}}\right]$ $\bar{\zeta} = \frac{3}{4}\sqrt{\pi\bar{\sigma}}, \quad \text{var}(\zeta) = \left(1 - \frac{9}{32}\pi\right)\bar{\sigma}$	Central Rayleigh distribution of degree 4
Chi-square of degree $2m$, Weinstock	$p_\zeta(\zeta) = \frac{2\zeta m}{\Gamma(m)\bar{\sigma}} \left(\frac{m\zeta^2}{\bar{\sigma}}\right)^{m-1} \exp\left[-\frac{m\zeta^2}{\bar{\sigma}}\right]$ $\bar{\zeta} = \sqrt{\frac{\bar{\sigma}}{m}}, \quad \text{var}(\zeta) = \bar{\sigma} \left\{1 - \frac{1}{m} [\Gamma(m + 0.5)/\Gamma(m)]^2\right\}$	Central Rayleigh distribution of degree $2m$
Rice or Rician, noncentral chi-square of degree 2	$p_\zeta(\zeta) = \frac{2\zeta(1+a^2)}{\bar{\sigma}} \exp\left[-a^2 - \frac{\zeta^2}{\bar{\sigma}}(1+a^2)\right] I_0\left(2a\zeta\sqrt{(1+a^2)/\bar{\sigma}}\right)$ $\bar{\zeta} = \frac{1}{2}\sqrt{\frac{\pi\bar{\sigma}}{1+a^2}} e^{-a^2} {}_1F_1[1.5, 1; a^2]$ $\text{var}(\zeta) = \left(\frac{\bar{\sigma}}{1+a^2}\right) e^{-a^2} \left[{}_1F_1(2, 1; a^2) - \frac{\pi}{4} e^{-a^2} {}_1F_1^2(1.5, 1; a^2) \right]$	Noncentral Rayleigh distribution of degree 2. ${}_1F_1(\cdot)$ is the confluent hypergeometric function.
Weibull	$p_\zeta(\zeta) = 2CB\zeta^{2C-1} \exp[-B\zeta^{2C}]$ $\bar{\zeta} = \Gamma(1+1/2C)B^{-1/2C}$ $\text{var}(\zeta) = [\Gamma(1+1/C) - \Gamma^2(1+1/2C)]B^{-1/2C}$	Also Weibull, one parameter (C) changed.
Log-normal	$p_\zeta(\zeta) = \frac{2}{\sqrt{2\pi}s\zeta} \exp\left[-2\ln^2(\zeta/\sqrt{\sigma_m})^2/s^2\right]$ $\bar{\zeta} = \sqrt{\sigma_m} \exp(s^2/8)$ $\text{var}(\zeta) = \sigma_m \exp(s^2/4)[\exp(s^2/4) - 1]$	Also log-normal, both parameters (s, σ_m) changed.

is caused by the “internal motion” of the clutter, such as the wave motion on the sea surface or the blowing leaves and limbs of the trees. Decorrelation is therefore unavoidable, and the rate of decorrelation is influenced by factors external to the radar such as wind speed. Range or aspect changes also induce decorrelation of clutter signatures.

Although the behavior of real targets can be quite complex, a sense of the change in frequency and angle required to decorrelate a target or clutter patch can be obtained by the following simple argument.

Consider a target consisting of a uniform line array of point scatterers tilted at an angle θ with respect to the antenna boresight and separated by Δx from one another, as shown in Fig. 2.12. For simplicity, assume an odd number $2M+1$ of scatterers indexed from $-M$ to $+M$ as shown. If the nominal distance to the radar R_0 is much larger than the target extent (that is, $R_0 \gg (2M+1)\Delta x$), then the range to the n th scatterer is approximately

$$R_n \approx R_0 + n \Delta x \sin \theta \quad (2.56)$$

If the target is illuminated with the waveform $A e^{j\Omega t}$, the received signal is

$$\begin{aligned} \bar{y}(t) &= \sum_{n=-M}^M A e^{j\Omega(t-2R_n/c)} \\ &= A e^{j\Omega(t-2R_0/c)} \sum_{n=-M}^M e^{-j4\pi n \Delta x \sin \theta F/c} \end{aligned} \quad (2.57)$$

To simplify the notation, define

$$z = F \sin \theta \quad \alpha = 4\pi \Delta x / c \quad (2.58)$$

Then $\bar{y}(t)$ can be considered as a function $\bar{y}(t; z)$ of both t and z . The correlation in the variable z is of interest, which includes both aspect angle and

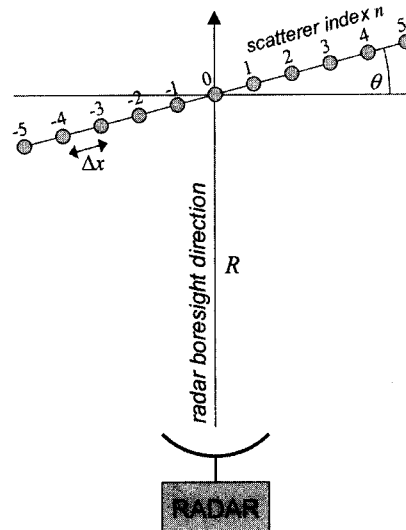


Figure 2.12 Geometry for calculation of RCS correlation length in frequency and aspect angle.

frequency. Note that $\bar{y}(t; z)$ is periodic in z with period $2\pi/\alpha$. The deterministic autocorrelation function is therefore

$$\begin{aligned}s_{\bar{y}}(\Delta z) &= \int_{-\pi/\alpha}^{\pi/\alpha} \bar{y}(t; z)\bar{y}^*(t; z + \Delta z) dz \\ &= \int_{-\pi/\alpha}^{\pi/\alpha} \left[A^* e^{j\Omega(t-2R_0/c)} \sum_{n=-M}^M e^{-j\alpha z n} \right] \left[e^{-j\Omega(t-2R_0/c)} \sum_{l=-M}^M e^{+j\alpha(z+\Delta z)l} \right] dz\end{aligned}\quad (2.59)$$

The complex exponential terms outside the summations cancel. Interchanging integration and summation and collecting terms then gives

$$s_{\bar{y}}(\Delta z) = |A|^2 \sum_{l=-M}^M e^{+j\alpha \Delta z l} \sum_{n=-M}^M \left[\int_{z=-\pi/\alpha}^{\pi/\alpha} e^{-j\alpha(n-l)z} dz \right] \quad (2.60)$$

A change of variables $z' = \alpha z$ makes it clear that the integral has the form of the inverse discrete-time Fourier transform of a constant spectrum $S(\Omega) = 2\pi/\alpha$. Therefore, the integral is just the discrete impulse function $(2\pi/\alpha)\delta_D[n - l]$. Using this fact reduces Eq. (2.60) to a single summation over l that can be evaluated to give

$$s_{\bar{y}}(\Delta z) = \frac{2\pi|A|^2}{\alpha} \frac{\sin[\alpha(2M+1)\Delta z/2]}{\sin[\alpha\Delta z/2]} \quad (2.61)$$

The correlation length can now be determined by evaluating Eq. (2.61) to find the value of Δz which reduces s to a given level. This value of Δz can then be converted into equivalent changes in frequency or aspect angle.

One criterion is to choose the value of Δz corresponding to the first zero of the correlation function. This occurs when the argument of the numerator equals π . Using Eq. (2.58) and defining the target length $L = (2M+1)\Delta x$,

$$\pi = \frac{4\pi \Delta x(2M+1)\Delta z}{2c} \Rightarrow \Delta z = \frac{c}{2L} \quad (2.62)$$

Recall that $z = F \sin \theta$. To determine the decorrelation length in angle, fix the transmitted frequency F so that $\Delta z = F(\Delta \sin \theta)$. Assuming θ is small (i.e., the radar is near broadside), $\Delta \sin \theta \approx \Delta \theta$. Equation (2.62) then becomes the desired result for the change in angle required to decorrelate the echo amplitude:

$$\Delta \theta = \frac{c}{2LF} \quad (2.63)$$

The frequency step required to decorrelate the target is obtained by fixing the aspect angle θ so that $\Delta z = \Delta F \sin \theta$. The result is

$$\Delta F = \frac{c}{2L \sin \theta} \quad (2.64)$$

This is minimum when $\theta = 90^\circ$. Note that $L \sin \theta$ is the length of the target projected along the radar boresight.

As an example, consider a target the size of an automobile, about 5 m long. At L band (1 GHz), the target signature can be expected to decorrelate in $(3 \times 10^8)/(2 \times 5 \times 10^9) = 30$ mrad of aspect angle rotation, about 1.7° , while at W band (95 GHz), this is reduced to only 0.018° . The frequency step required for decorrelation with an aspect angle of 45° is 42.4 MHz. This result does not depend on the transmitted frequency.

The results of Eqs. (2.63) and (2.64) are based on a highly simplified target model and an assumption about what constitutes “decorrelation.” For example, defining “decorrelation” to be the point at which the correlation function s first drops to $1/2$ or $1/e$ of its peak results in a smaller estimate of the required change in angle or frequency to decorrelate the target. Also, as will be seen in Chap. 6, many radars operate on the magnitude-squared of the echo amplitude, rather than the magnitude as has been assumed in this derivation. A square law detector produces a correlation function proportional to the square of Eq. (2.61) (Birkmeier and Wallace, 1963). The first zero therefore occurs at the same value of Δz , and the previous conclusions still apply. However, if a different definition of decorrelation is used (such as the 50 percent decorrelation point), the required change in Δz is less for the square law than for the linear detector.

For rigid targets, the amount of aspect angle rotation required to decorrelate the target echoes can be estimated from Eq. (2.63). The corresponding amount of time required to decorrelate successive measurements depends on the geometry of the radar/target encounter and their relative velocity. It is seen in the next section that target echo amplitudes are represented by statistical models that involve a choice of both a pdf for the target echoes and an assumption about the degree of correlation between successive measurements. It is shown in Chap. 6 that the correlation time assumption significantly affects estimates of detection performance.

It is also seen in Chap. 6 that in most cases, detection performance is improved when successive target echoes are uncorrelated. For this reason, some radars use a technique called *frequency agility* to force decorrelation of successive measurements (Ray, 1966). In this process, the radar frequency is increased by ΔF hertz or more between successive pulses, where ΔF is given by Eq. (2.64), ensuring that the target echo decorrelates from one pulse to the next. Once the desired number of samples is obtained, the cycle of increasing frequencies is repeated for the next set of measurements.

2.2.6 Swerling models

An extensive body of radar detection theory results have been built up using the four *Swerling models* of target RCS fluctuation (Swerling, 1960; Meyer and Mayer, 1973; Nathanson, 1991; Skolnik, 2001). Swerling models are intended to address the common problem of making a detection decision based not on one, but on a block of M echo samples from a given resolution cell. One motivation for considering detection based on a block of M samples may have originally been based on a simplified model of the operation of a surveillance radar, such

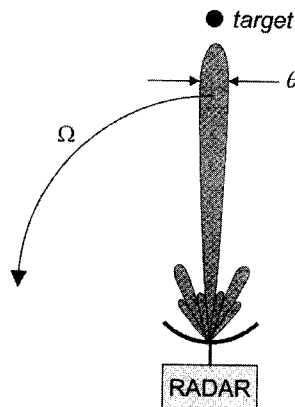


Figure 2.13 Rotating antenna rationale for Swerling model decorrelation assumptions.

as might be used to detect aircraft. Consider a radar with an antenna that rotates at a constant angular velocity Ω radians per second with an azimuth beamwidth of θ radians and a pulse repetition frequency of PRF hertz. Suppose that a target is present at a particular location. The geometry is shown in Fig. 2.13. Although some echo energy from the target is received on every pulse through the antenna side lobes, significant returns are received only when the target is in the antenna main lobe. Every complete 360° sweep of the antenna results in a new set of $M = (\theta/\Omega)PRF$ mainbeam pulses.

This is not the only way a block of related pulse echoes can arise. Many modern systems are designed to transmit bursts of pulses at a constant PRF, often with the antenna staring in a fixed direction. The time interval required for this measurement, which is simply M/PRF , is called a *coherent processing interval* (CPI).[†] The system may then repeat the entire measurement in the same or a different look direction, change the PRF to make a related measurement, or make any of a number of other changes in collecting the next CPI of data. As is seen in Chap. 4, the M -pulse burst is a common waveform well-suited to Doppler measurements, adaptive interference suppression, and imaging applications.

Each Swerling model is a combination of a probability density function and a decorrelation time for the RCS σ . They are formed from the four combinations of two choices for the pdf and two for the decorrelation time. Swerling considered two extreme cases for the correlation properties of this block of M measurements of σ . The first assumes they are all perfectly correlated, so that all M pulses collected on one sweep have the same value. The M new pulses collected on the next antenna sweep all have the same value as one another also, but their value is independent of the value measured on the first sweep.

[†]The term “CPI” is often used to refer to the block of data samples collected within the time interval, as well as to the time interval itself.

This case is referred to as *scan-to-scan decorrelation*. The second case assumes that each individual pulse on each sweep results in an independent value for σ . This case is referred to as *pulse-to-pulse decorrelation*.

The two density functions used by Swerling to describe RCS are the Rayleigh/exponential and the chi-square of degree four (see Table 2.3). The Rayleigh model describes the behavior of a complex target consisting of many scatterers, none of which is dominant. The fourth-degree chi-square models targets having many scatterers of similar strength with one dominant scatterer. Although the Rice distribution with $a^2 = 1$ is the exact pdf for this case, the chi-square is an approximation that is more analytically tractable. The approximation of the Rice distribution by the fourth-degree chi-square is based on matching the first two moments of the two pdfs (Meyer and Mayer, 1973). These moments match when the RCS of the dominant scatterer is $1 + \sqrt{2} = 2.414$ times that of the sum of the RCS of the small scatterers, so the fourth-degree chi-square model fits best for this case. More generally, a chi-square of degree $2m = 1 + [a^2/(1+2a)]$ is a good approximation to a Rice distribution with a ratio of a^2 of the dominant scatterer to the sum of the small scatterers; this is readily seen using the mean and variance formulas for the two distributions given in Table 2.3. However, only the specific case of the fourth-degree chi-square is considered a Swerling model.

The Swerling models are the four combinations of the two choices for the pdf of σ and the two choices for the decorrelation characteristics. The models are denoted as “Swerling 1,” “Swerling 2,” and so forth. Table 2.5 defines the four cases. In some sources, the nonfluctuating target is identified as the “Swerling 0” or “Swerling 5” model.

Figures 2.14 and 2.15 illustrate the difference in the behavior of two of the Swerling models. In both cases, the received power from a single point scatterer for 500 samples of a unit mean Swerling RCS is plotted, and in both it is assumed that 10 samples are obtained on each scan of the radar, while no echo is received when the point target is outside the beam. Figure 2.14 is a sample Swerling 1 (exponential pdf, scan-to-scan decorrelation) series. The scan-to-scan decorrelation implies that all 10 samples within a single scan are identical, but independent of the 10 received on the next scan. In contrast, Fig. 2.15 illustrates a Swerling 4 case (chi-square pdf, pulse-to-pulse decorrelation) in which each individual sample is independent of the others.

TABLE 2.5 Swerling Models

Probability density function of RCS	Decorrelation	
	Scan-to-scan	Pulse-to-pulse
Rayleigh/exponential	Case 1	Case 2
Chi-square, degree 4	Case 3	Case 4

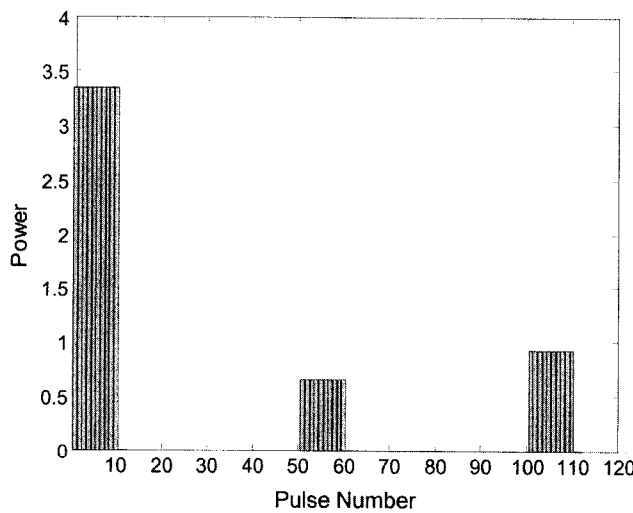


Figure 2.14 500 samples of a unit mean Swerling 1 power sequence with a 10-sample scan time.

2.3 Clutter

The term *clutter* implies an interference signal, but in radar it refers to a component of the received signal due to echoes from volume or surface scatterers. Such scatterers include the earth's surface, including both terrain and sea; weather echoes (for example, rain clouds); and man-made distributed clutter, such as

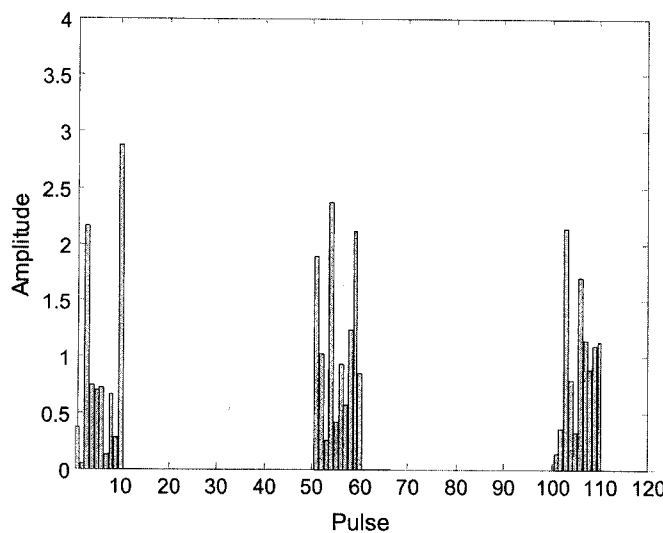


Figure 2.15 500 samples of a unit mean Swerling 4 power sequence.

so-called *chaff* clouds of airborne scatterers, typically made out of lightweight strips of reflecting material. Clutter echoes differ from targets and noise in that they are sometimes interference and sometimes the desired signal. For instance, synthetic aperture imaging radars are designed to image the earth surface, thus the terrain is the target in a SAR radar. For an airborne or spaceborne surveillance radar trying to detect moving vehicles on the ground, the surrounding terrain echo is an interference signal.

From a signal processing point of view, the major concern is how to model clutter echoes. As with man-made targets, terrain is a complex target and the echoes are highly sensitive to radar parameters and aspect angle. Thus, clutter is also modeled as a random process. Clutter differs from noise in two major ways: its power spectrum is not white (i.e., it is correlated interference), and, since it is the result of echo, the power is affected by such radar and scenario parameters as the antenna gain, transmitted power, signal processing gain, and the range from the radar to the terrain. In addition to temporal correlation, clutter can also exhibit spatial correlation: the reflectivity samples from adjacent resolution cells may be correlated. Two excellent general references on land and sea clutter phenomenology are books by Ulaby and Dotson (1989) and Long (2001).

2.3.1 Behavior of σ^0

Area clutter (land and sea surface) is of the most interest. Area clutter reflectivity is characterized by its mean or median value of radar cross section, σ^0 (dimensionless) and the probability density function of the reflectivity variations. For a given value of mean or median σ^0 , many of the same pdfs described in Sec. 2.2.4 are applied to modeling clutter as well. Popular examples include Rayleigh/exponential, log-normal, and Weibull distributions.

The nature of terrain observed by the radar varies with spatial location, weather, engagement geometry, and other factors. Consequently, selection of a pdf is not sufficient to model clutter. It is also necessary to model the dependence of σ^0 on these parameters. First consider land clutter. σ^0 is a strong function of terrain type, wavelength, polarization, grazing angle, surface roughness, and moisture, to name a few parameters. Values of σ^0 commonly range from -60 to -10 dB. Extensive measurement programs over the years have collected statistics of land clutter under various conditions and resulted in many tabulations of σ^0 for various terrain types and conditions, as well as models for the variation of σ^0 . One particular concern has been characterizing the variation of σ^0 with grazing angle δ . Generally, σ^0 decreases rapidly at very low grazing angles, and increases rapidly at very high grazing angles (radar look direction normal to the clutter surface), with a milder variation of σ^0 with grazing angle in a middle “plateau region.” Figure 2.16 is a notional diagram of this behavior.

One of the most popular models for the behavior of σ^0 is the “constant gamma” model (Long, 2001):

$$\sigma^0 = \gamma \sin \delta \quad (2.65)$$

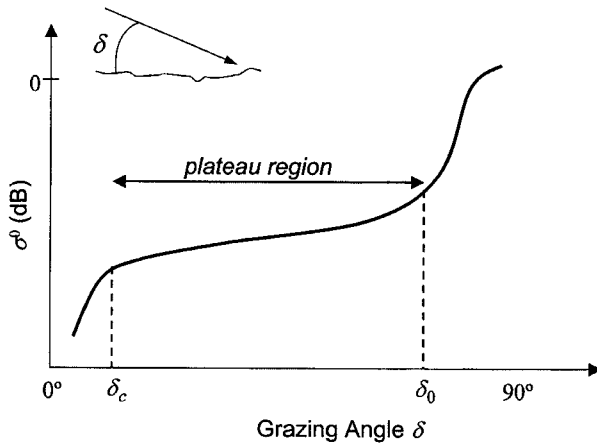


Figure 2.16 General behavior of σ^0 with grazing angle for land clutter. (After Long, 2001.)

where γ is a characteristic of the particular clutter type at the radar frequency and polarization of interest. This model predicts a maximum value of σ^0 at normal incidence and σ^0 vanishing as the grazing angle tends to zero. However, it does not accurately reflect the sharp increase in σ^0 at near-normal incidence angles, and additional models are often used at the two extremes of near-grazing and near-normal incidence.

2.3.2 Signal-to-clutter ratio

In many scenarios, the dominant interference is not noise, but clutter. Consequently, the *signal-to-clutter ratio* (SCR) is often of more importance than the *signal-to-noise* (SNR) ratio. The SCR is easily obtained as the ratio of the received signal power, given by Eq. (2.11) to the received clutter power, given by Eq. (2.25), (2.30), or (2.32) for the volume clutter, beam-limited area clutter, and pulse-limited area clutter cases, respectively. The resulting equations are

$$\begin{aligned} \text{SCR} &= \frac{\sigma}{R^2 \eta \Delta R \theta_3 \phi_3} && \text{(volume clutter case)} \\ &= \frac{\sigma \sin \delta}{R^2 \phi_3 \theta_3 \sigma^0} && \text{(beam-limited area clutter case)} \\ &= \frac{\sigma \cos \delta}{R^3 \sigma^0 \Delta R \theta_3} && \text{(pulse-limited area clutter case)} \end{aligned} \quad (2.66)$$

In each case, such system parameters as the transmitted power and the antenna gain cancel out. This occurs because both the clutter and target signals are echoes of the radar pulse; increasing power or antenna gain increases the strength of both types of echoes equally. Thus, the SCR just becomes the ratio of the target RCS to the total RCS of the contributing clutter.

2.3.3 Temporal and spatial correlation of clutter

Clutter decorrelation in time is induced by internal motion for clutter, such as leaves moving in the wind on trees or waves on the sea surface, and by changes in radar-target geometry for both clutter and targets. Various investigators have experimentally characterized the decorrelation characteristics of clutter echoes due to internal motion, or equivalently, their power spectrum. For example, one model suggested to estimate the power spectrum of the RCS of foliated trees or rain uses a cubic spectrum (Currie, 1987):

$$S_\sigma(F) = \frac{A}{1 + (F/F_c)^3} \quad (2.67)$$

The corner frequency F_c is a function of the wavelength and either wind speed (for trees) or rain rate (for rain). Some sample measured values are given in Table 2.6. Another model frequently used to model generic power spectra is the Gaussian given by

$$S_\sigma(F) = A \exp \left[-\alpha \left(\frac{F}{F_0} \right)^2 \right] \quad (2.68)$$

The Gaussian model is very commonly used in weather radar, and is the basis of the pulse pair Doppler velocity estimation technique discussed in Chap. 5.

Haykin et al. show that both the cubic and Gaussian power spectral models can be well matched by a low-order autoregressive (AR, or all-pole) spectrum model of the form (Haykin, Currie, and Kessler, 1982)

$$S_\sigma(F) = \frac{A}{1 + \sum_{k=1}^N \alpha_k F^{2k}} \quad (2.69)$$

Real clutter measured from ground-based radars appears to be well matched using an order N of only two to four (Haykin, Currie, and Kessler, 1982). Other studies of clutter measured by airborne radars in a landing scenario indicate that orders up to 10 may be required (Baxa, 1991). The AR clutter spectrum model has the advantage that its parameters can be computed directly from

TABLE 2.6 Cubic Power Spectrum Corner Frequencies (Hz) for Rain and Tree Clutter

Target	Radar frequency, GHz		
	10	35	95
Rain, 5 mm/hr	35	80	140
Rain, 100 mm hr	70	120	500
Trees, 6-15 mph wind	9	21	35

SOURCE: Currie, N. C. "Clutter Characteristics and Effects," chapter 10 in J. L. Eaves and K. E. Reedy (eds.), *Principles of Modern Radar*. Van Nostrand Reinhold, New York, 1987.

measured data and adapted in real time using the Levinson-Durbin or similar algorithms (Kay, 1988). Furthermore, the AR parameters can be used to construct optimal adaptive clutter suppression filters, as is seen in Chap. 5. The disadvantage is that the calculations rapidly become computationally intensive as the model increases.

2.3.4 Compound models of radar cross section

As is seen in Chap. 6, radar detection performance predictions depend strongly on the details of target and clutter RCS models. Furthermore, it is well known that RCS statistics vary significantly with a host of factors such as geometry, resolution, wavelength, and polarization. Consequently, the development of good statistical RCS models is a very active area of empirical and analytical research. Following are three brief examples of an extension to the basic modeling approach described earlier, all motivated by the complexities of modeling clutter.

Some RCS probability density functions are physically motivated, especially the Rayleigh/exponential model (which follows from a central limit theorem argument) and the Rice model (which corresponds to a Rayleigh model with an additional dominant scattering source). Others, such as the lognormal or Weibull, have been developed empirically by fitting distributions to measured data. One attempt to provide a physical justification for a non-Rayleigh model abandons the single-pdf approach, instead assuming that the random variable representing echo amplitude (voltage) can be written as the product of two independent random variables:

$$\zeta = xy \quad (2.70)$$

The pdf of ζ can then be represented in a Bayesian formulation as

$$p_\zeta(\zeta) = p_x(x)p_{\zeta|x}(\zeta|x) \quad (2.71)$$

Ward uses this model to describe sea clutter (Ward, 1981). He identifies the random variable x with a slowly decorrelating component having a voltage distribution following a chi-square of degree $2m$ with $m \geq 2.5$. This component is introduced to account for “bunching” of scatterers due to ocean swell structure and radar geometry, and represents variation in the mean of the voltage over time. The distribution $p_{\zeta|x}(\zeta|x)$ is assumed to represent the composite of a large number of independent scatterers. Its voltage distribution is therefore Rayleigh. The overall pdf $p_\zeta(\zeta)$ can be shown to be the *K-distribution*, which had previously been proposed as a model of sea clutter (Jakeman and Pusey, 1976). Thus, the product formulation suggests that modulation of a standard Rayleigh variable by a chi-square distributed geometric term can account for observed sea clutter distributions.

More recent research has begun to bridge the gap between the physics of scattering and the apparent success of compound clutter models of the type promoted by Ward and Jakeman and Pusey. Sangston summarizes the work

that considers an extension of the “many scatterer” physical model that leads to the Rayleigh distribution (Sangston, 1997). Specifically, consider the model of Eq. (2.50), but with the fixed number of scatterers N replaced by a random variable N

$$\zeta = \left| \sum_{i=1}^N \sqrt{\sigma_i} e^{-j4\pi R_i/\lambda} \right| \quad (2.72)$$

This representation is referred to as a “number fluctuations” model. Depending on the choice of the statistics of the number N of scatterers contributing to the return at any given time, the model of Eq. (2.72) can result in K , Weibull, gamma, Nakagami- m , or any of a number of other distributions in the class of so-called Rayleigh mixtures (Sangston, 1997).

Much of the work in compound RCS models has been performed in the context of sea clutter analysis, and empirical sea clutter data have often been observed to exhibit non-Rayleigh statistics such as Weibull, K , and log-normal distributions. The number fluctuation model is intuitively appealing in this case, because it can be related to the physical behavior of waves. Specifically, scattering theory suggests that the principal scatterers on the ocean surface are the small capillary waves, as opposed to the large swells, and that these small scattering centers tend to cluster near the crest of the swells, with fewer of them in between. In other words, they are nonuniformly distributed over the sea surface (Sangston, 1997). Consequently, a radar illuminating the sea will receive echoes from a variable number N of scatterers as the crests of the swells move into and out of a given resolution cell. Thus the success of the number fluctuation model, which sums echoes from a variable number of scatterers, in predicting Weibull and K distributions provides a link between a phenomenological model of sea scatter and empirically observed statistics.

All of the statistical models described in Sec. 2.2.4 apply to the scattering observed from a single resolution cell, i.e., they represent the variations in RCS observed by measuring the same region of physical space multiple times, e.g., by transmitting multiple pulses in the same direction and measuring the received power at the same delay after each transmission. Another use of the product model of Eq. (2.70) and (2.71) is to describe the spatial variation of clutter reflectivity. If the scene being viewed by the radar is nonhomogenous, then the characteristics of the RCS observed in one resolution cell might vary significantly from those of another. For example, the dominant clutter observed by a scanning radar at a coastal site might be an urban area in one look direction and the sea in another. Another example occurs when scattered rain cells occupy only part of the scanned region, so that some resolution cells contain rain while others are clear.

This situation can be modeled by letting the slowly decorrelating term x in the product model represent spatial variations in the local mean of the received voltage. If the pdf of x is log-normal with a large variance and the pdf of ζ conditioned on x is gamma distributed (which includes Rayleigh as a special case),

then the overall pdf of the product ζ has a log-normal distribution (Lewinski, 1983). Consequently, the product model implies that log-normal variations of the local mean from one resolution cell to another could account for the log-normal variation often used to model ground clutter returns. A similar argument can be used to justify the log-normal model for target RCS by modeling the variation of RCS with aspect angle as a log-normal process.

2.4 Noise Model and Signal-to-Noise Ratio

The echo signal received from a target or clutter inevitably competes with noise. There are two sources of noise: that received through the antenna from external sources, and that generated in the radar receiver itself.

External noise is a strong function of the direction in which the radar antenna is pointed. The primary contributor is the sun. If the antenna is directed toward the night sky and there are no interfering microwave sources, the primary source is *galactic* (also called *cosmic*) noise. Internal noise sources include *thermal noise* (also called *Johnson noise*) due to ohmic losses, *shot noise* and *partition noise* due to the quantum nature of electric current, and *flicker noise* due to surface leakage effects in conducting and semiconducting devices (Carlson, 1976).

Of these various sources, thermal noise is normally dominant. The theories of statistical and quantum mechanics dictate that thermal noise voltage in an electronic circuit is a zero-mean Gaussian random process (Curlander and McDonough, 1991). The mean energy of the random process is $kT/2$ joules, where T is the temperature of the noise source in degrees Kelvin (absolute temperature) and $k = 1.38 \times 10^{-23}$ J/K is *Boltzmann's constant*. The power spectrum $S_n(F)$ of the thermal noise delivered to a matched load is

$$S_n(F) = \frac{hF}{\exp(hF/kT) - 1} \quad \text{W/Hz} \quad (2.73)$$

(Ziemer and Tranter, 1976) where $h = 6.6254 \times 10^{-34}$ J/s is *Planck's constant*. If $hF/kT \ll 1$, a series approximation gives $\exp(hF/kT) \approx 1 + hF/kT$ so that Eq. (2.73) reduces to the white noise spectrum

$$S_n(F) = kT \quad \text{W/Hz} \quad (2.74)$$

Note that Eq. (2.74), when integrated over frequency, implies infinite power in the white noise process. In reality, however, the noise is not white (Eq. (2.73)) and, in any event, it is observed in any real system only over a finite bandwidth. For frequencies below 100 GHz, the approximation of Eq. (2.74) requires the effective noise temperature T (to be defined below) to be larger than about 50K, which is almost always the case. Consequently, thermal noise has a white power spectrum. For many practical systems, it is reasonable to choose the temperature of the system to be the "standard" temperature $T_0 = 290\text{K}$. In this case, $kT_0 \approx 4 \times 10^{-21}$ W/Hz.

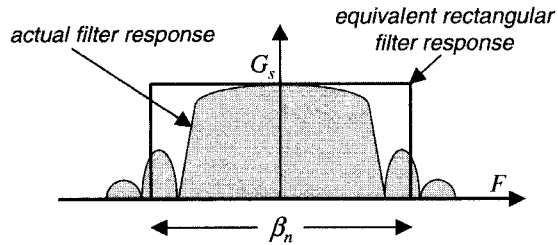


Figure 2.17 Illustration of the concept of noise equivalent bandwidth of a filter.

In a coherent radar receiver, the noise present at the front end of the system contributes noise to both the I and Q channels after the quadrature demodulation. It is easy to show (Ziemer and Tranter, 1976) that the I and Q channel noises are both zero-mean Gaussian random processes with equal power. Since the total noise spectral density is kT watts per hertz, the noise density in each channel individually is $kT/2$ watts per hertz. Furthermore, if the power spectrum of the input noise is white, then the I and Q noise processes are uncorrelated and their power spectra are also white. Since the I and Q noise processes are Gaussian and uncorrelated, it follows that they are also independent (Papoulis, 1984). Finally, since the I and Q signals are independent zero-mean Gaussian processes, it also follows that the magnitude of the complex signal $I + jQ$ is Rayleigh distributed, the magnitude-squared is exponentially distributed, and the phase angle $\tan^{-1}(Q/I)$ is uniformly distributed over $(0, 2\pi]$ as described in Sec. 2.2.5.

Radar receivers do not have infinite bandwidth. The bandwidth of the various components of a receiver varies, but the narrowest bandwidth is generally approximately equal to the bandwidth of the transmitted pulse. If the receiver contains any component of narrower bandwidth, signal energy will be lost, reducing sensitivity. If the most narrowband component has a bandwidth appreciably wider than the pulse bandwidth, the signal will have to compete against more noise power than necessary, again reducing sensitivity. Thus the frequency response of the receiver can be approximated as a bandpass filter centered at the transmit frequency, with a bandwidth equal to the waveform bandwidth.

Real filters do not have perfectly rectangular passbands. For analyzing noise power, the *noise-equivalent bandwidth* β_n of a filter described by the transfer function $H(F)$ is used. Figure 2.17 illustrates the concept. The noise equivalent bandwidth is the width an ideal rectangular filter, with gain equal to the peak gain of the actual filter, must have so that the area under the two squared frequency responses are equal. This condition guarantees that given a white noise input, both filters exhibit the same output noise power. Thus

$$\beta_n = \frac{\int_{-\infty}^{\infty} |H(F)|^2 dF}{\max[|H(F)|^2]} = \frac{1}{G_s} \int_{-\infty}^{\infty} |H(F)|^2 dF \quad (2.75)$$

where G_s is defined as the maximum gain of $H(F)$. The total noise power N present at the output of the filter $H(F)$ is then given by

$$\begin{aligned} N &= \int_{-\infty}^{\infty} |H(F)|^2 S_n(F) dF \\ &= kT \int_{-\infty}^{\infty} |H(F)|^2 dF \\ &= kT \beta_n G_s \end{aligned} \quad (2.76)$$

White noise passed through a filter $H(F)$ is no longer white, but instead has the power spectrum $|H(F)|^2$. If $|H(F)|^2$ is modeled as a rectangular filter of two-sided bandwidth β_n hertz, the autocorrelation function of the noise at the filter output is a sinc function with its first zero at delay $1/\beta_n$ seconds. Thus, the receiver output noise is not white, and its decorrelation time is on the order of $1/\beta_n$ seconds. However, it will be seen in Chap. 3 that the receiver output is normally sampled at intervals of approximately $1/\beta_n$ seconds. Consequently, the noise component of the successive receiver output samples are still uncorrelated with one another.

The power spectral density at the output of any noise source or circuit can be described as the product of Boltzmann's constant and some equivalent temperature T' , mimicking the simple formulation of Eq. (2.74). Source noise power is usually referenced to the input of a system, so that the power gain G_s (or loss, in which case $G_s < 1$) of the system must also be taken into account. That is, if the observed output power spectral density (still assumed white) is some value S_n , then an equivalent temperature T' of the noise source is defined to be

$$T' \equiv \frac{S_n}{kG_s} \quad (2.77)$$

so that $S_n = kT'G_s$ and the total noise power, using Eq. (2.76) is

$$N = kT' \beta_n G_s \quad (2.78)$$

The total output noise power at the receiver output is the primary quantity of interest. In a radar system, the contributors to this noise include the external noise, the intrinsic $kT_0\beta_n$ thermal noise, and additional thermal noise due to losses in the antenna structure and nonideal receivers. Detailed noise analyses assign individual equivalent noise temperatures to each stage in the system; good introductory description was given by Curlander and McDonough (1991). When considering the system as a whole, it is common to express the total output noise power as the sum of the power that would be observed due to the minimum noise density kT_0 at the input and a second term that accounts for the additional noise due to the nonideal system

$$N = kT_0\beta_n G_s + kT_e\beta_n G_s \quad (2.79)$$

In this equation, G_s is now the power gain of the complete receiver system, including antenna loss effects. The equivalent temperature T_e used to account for noise above the theoretical minimum is called the *effective temperature* of the system.

The noise temperature description of noise power is most useful for low-noise receivers. An alternative description common in radar is based on the idea of *noise figure* F_n , which is the ratio of the actual noise power at the output of a system to the minimum power $kT_0\beta_nG_s$ (Skolnik, 1980). As with noise temperatures, various noise figures can be defined to include the effects of just the receiver, or of the entire antenna and receiver system, and so forth. Here, the term *noise figure* used without qualification will mean the noise figure of the complete receiver system, so that

$$F_n = \frac{N}{kT_0\beta_nG_s} \quad (2.80)$$

Equation (2.80) implies that knowledge of the noise equivalent bandwidth and gain of the receiver system are sufficient to calculate the output noise power using $N = kT_0\beta_nF_nG_s$. It also follows from using Eq. (2.79) in Eq. (2.80) that $T_e = (F_n - 1)T_0$. Typical noise figures for radars can be as low as 2 or 3 dB, and as high as 10 dB or more. Corresponding effective temperatures range from about 170K to over 2600K.

In Sec. 2.2, the term “radar range equation” was applied to Eqs. (2.11), (2.25), (2.30), and (2.32). These expressions described the power received by the radar given various system and propagation conditions. As will be seen in Chap. 6, the detection performance of a radar depends not on the received power per se but on the SNR at the point of detection. The earlier results can be used to convert the power range equations to SNR range equations.

To illustrate, consider the point target range Eq. (2.11), which expresses the power P_r of the signal available at the input to the receiver. The signal power at the output will be $P_o = G_sP_r$ provided the signal bandwidth is entirely contained within the receiver bandwidth B_n . From Eq. (2.80), the output noise power is $N_o = kT_0\beta_nF_nG_s$. The signal to noise ratio is therefore

$$\begin{aligned} \chi &= \frac{P_o}{N_o} \\ &= \frac{G_s P_t G^2 \lambda^2 \sigma}{(4\pi)^3 R^4 L_s L_a(R)} \cdot \frac{1}{k T_0 \beta_n F_n G_s} \\ &= \frac{P_t G^2 \lambda^2 \sigma}{(4\pi)^3 R^4 k T_0 \beta_n F_n L_s L_a(R)} \end{aligned} \quad (2.81)$$

The last expression in Eq. (2.81) gives the SNR in terms of transmitter and receiver characteristics, target RCS, range, and loss factors. Modifications of Eqs. (2.25), (2.30), and (2.32) for volume and area scatterers to express them in terms of signal to noise ratio are obtained in the same manner by simply adding the term $kT_0\beta_nF_n$ to their denominators.

Like Eq. (2.11), Eq. (2.81) is also often called the radar range equation. In the remainder of this text, the term “range equation” or “radar range equation” refers to the SNR form of Eq. (2.81) and its analogues for volume and area scatterers.

2.5 Jamming

Jamming refers to intentional interference directed at the radar system from a hostile emitter. Jamming is an example of *electronic countermeasures* (ECM) or *electronic attack* (EA). As noted earlier, the purpose of most radar signal processing is to improve the SIR of the data before a detection test is carried out. The purpose of jamming is just the opposite: to reduce the SIR so that the detection performance of the radar is degraded.

The most basic form of jamming is simple noise jamming. A hostile emitter directs an amplified noise waveform at the victim radar, essentially increasing the noise level out of the receiver. If the noise power spectrum fills the entire radar receiver bandwidth, then the noise out of the receiver will appear like any other white noise process and is modeled in the same way. More advanced forms of noise jamming use various amplitude and frequency modulations. Instead of noise, other jamming techniques use waveforms designed to mimic target echoes and fool the radar into detecting and tracking non-existent targets.

Even a limited discussion of ECM is out of the scope of this text, due both to the breadth of the topic and the limited amount of material publishable in the open literature. The reader is referred to the book by Lothes et al., (1990) for a good general reference on jamming signals in radar.

2.6 Frequency Models: The Doppler Shift

2.6.1 Doppler shift

If the radar and scatterer are not at rest with respect to one another, the frequency F_r of the received echo will differ from the transmitted frequency F_t due to the Doppler effect. A correct description of the Doppler shift for electromagnetic waves requires the theory of special relativity. Consider a monostatic radar, where the transmitter and receiver are at the same location and do not move with respect to one another. Suppose a scatterer in the radar field of view is moving with a velocity component v toward the radar. If the transmitted radar frequency is F_t , then the theory of special relativity predicts that the received frequency F_r will be (Temes, 1959; Gill, 1965)

$$F_r = \left(\frac{1 + v/c}{1 - v/c} \right) F_t \quad (2.82)$$

Thus, an approaching target causes an increase in the received frequency. Substituting $v = -v$ shows that a receding target decreases the received frequency. This is in keeping with our experience with the whistles of passing trains.

Equation (2.82) can be simplified without significant loss of precision because the velocity of actual radar targets is a small fraction of c . For example, the value of v/c for a supersonic aircraft traveling at Mach 2 (about 660 m/s) is only 2.2×10^{-6} . Expand the denominator of Eq. (2.82) in a binomial series:

$$\begin{aligned} F_r &= (1 + v/c)(1 - v/c)^{-1} F_t \\ &= (1 + v/c)[1 + (v/c) + (v/c)^2 + \dots] F_t \\ &= [1 + 2(v/c) + 2(v/c)^2 + \dots] F_t \end{aligned} \quad (2.83)$$

Discarding all second-order and higher terms in (v/c) leaves

$$F_r = [1 + 2(v/c)] F_t \quad (2.84)$$

The difference F_D between the transmitted and received frequencies is called the *Doppler frequency* or *Doppler shift*. For this case of an approaching target it is

$$F_D = +\frac{2v}{c} F_t = +\frac{2v}{\lambda_t} \quad (2.85)$$

where λ_t is the transmitted wavelength; for a receding target the Doppler shift would be equal in magnitude to Eq. (2.85), but negative. The magnitude of Eq. (2.85) is the expression conventionally used in radar to evaluate Doppler shift, with the sign determined by whether the radar and target are closing or opening in relative range.

The numerical values of Doppler shift are small compared to the RF frequencies. Table 2.7 gives the magnitude of the Doppler shift corresponding to a velocity of 1 m/s at various typical radar frequencies. The Mach 2 aircraft, observed with the L band radar, would cause a Doppler shift of only 4.4 kHz in a 1 GHz carrier frequency.

For a monostatic radar, the observed Doppler shift is proportional to the component of velocity in the direction of the radar, called the *radial velocity*. If the angle between the velocity vector of target traveling at v meters per second and the radar boresight is ψ , the radial velocity is $v \cos \psi$ meters per second. The geometry is illustrated in two dimensions in Fig. 2.18. The magnitude of the Doppler shift is maximum when the target is traveling directly toward or away from the radar. The Doppler shift is zero, regardless of the target velocity, when the target is crossing orthogonally to the radar boresight.

TABLE 2.7 Doppler Shift Resulting from a Velocity of 1 m/s

Band	Frequency (GHz)	Doppler shift (Hz) for $v = 1$ m/s
L	1	6.67
C	6	40.0
X	10	66.7
K _a	35	233
W	95	633

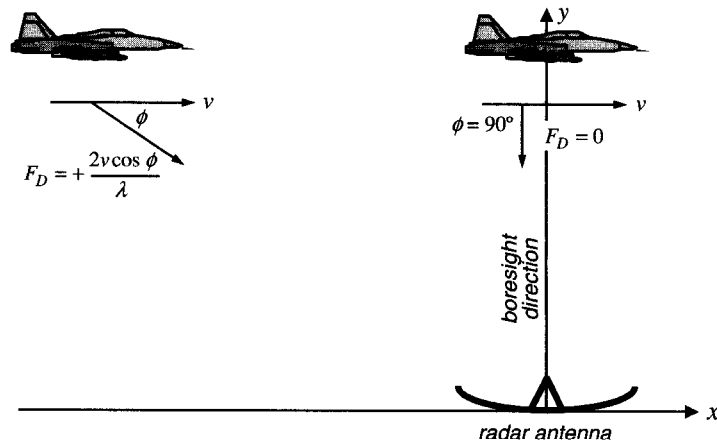


Figure 2.18 Doppler shift is determined by the radial component of relative velocity between the target and radar.

Radar waveforms are not pure monochromatic sinusoids, but instead have a finite bandwidth β_t . Applying Eq. (2.85) to the upper and lower frequency components shows that the Doppler shifted received bandwidth β_r is

$$\beta_r = [1 + 2(v/c)]\beta_t \quad (2.86)$$

Because the bandwidth is almost always 10 percent or less of the carrier frequency (and usually 1 percent or less), the change in bandwidth of $2(v/c)\beta_t$ is usually completely insignificant.

As mentioned earlier, the values of Doppler shift are quite small. As an example, consider a target moving at a velocity of 100 m/s (224 mi/h) with respect to an X band (10 GHz) radar. Using Eq. (2.85) or Table 2.7, the resulting Doppler shift will be 6.67 kHz. This Doppler shift is too small to be measured in a single pulse echo. Suppose the pulse length is 10 μ s. The frequency resolution available with a 10 μ s observation time is $1/(10 \mu\text{s}) = 100 \text{ kHz}$, much larger than that required to estimate the 6.67 kHz shift. Put another way, in 10 μ s a 6.67 kHz sinusoid progresses through only 6.67 percent of a cycle. For this reason, most radars cannot measure Doppler shifts of interest from a single pulse.

Despite the small values of Doppler shift, it will be seen in Sec. 2.6.3 that Doppler shifts are large enough to be detected. This will be accomplished by measuring phase shifts over multiple pulse repetition intervals (PRIs), giving a much longer observation timeline and thus much better Doppler resolution. These Doppler shifts can be used to advantage to detect echoes from moving targets in the presence of much stronger echoes from clutter or to drastically improve cross-range resolution. Uncompensated Doppler shifts can also have harmful effects, particularly a loss of sensitivity for some types of waveforms.

2.6.2 Simplified approach to Doppler shift

As argued in deriving Eq. (2.84), the relativistic effect on Doppler shift is insignificant for any realistic target velocity because v/c is so small. Classical derivations can therefore be used with no significant error (Gill, 1965). In the analysis so far, Doppler shift has been considered only for a sinusoid of infinite duration and a constant radial velocity v . A simple generalization of the Doppler shift formula can be developed that is easily applied to arbitrary motion between the radar and target and any waveform using a classical physics approach.

Suppose the one-way range from the radar to the target as a function of time is $R(t)$. If the transmitter radiates a signal $\bar{x}(t)$, the echo received will simply be (ignoring amplitude scaling factors) a delayed replica of the transmitted signal:

$$\bar{y}(t) = \bar{x}\left(t - \frac{2R(t)}{c}\right) \quad (2.87)$$

Though simple, Eq. (2.87) leads to correct descriptions of time-varying Doppler shifts. For example, suppose the signal $\bar{x}(t)$ is a simple pulse of the form

$$\bar{x}(t) = a(t) \exp(j2\pi F_t t) \quad (2.88)$$

where $a(t)$ is the pulse envelope. Now suppose the target is moving toward the radar at a constant radial velocity v . This means that

$$R(t) = R_0 - vt \quad (2.89)$$

where R_0 is the range at some time $t = 0$. Combining Eq. (2.87) through (2.89) gives the received signal as

$$\begin{aligned} \bar{y}(t) &= a\left(t - \frac{2(R_0 - vt)}{c}\right) \exp\left[j2\pi F_t\left(t - \frac{2(R_0 - vt)}{c}\right)\right] \\ &\approx a\left(t - \frac{2R_0}{c}\right) \exp\left(-j\frac{4\pi c}{\lambda_t} R_0\right) \exp\left[+j2\pi\left(\frac{2v}{\lambda_t}\right)t\right] \exp(j2\pi F_t t) \end{aligned} \quad (2.90)$$

In Eq. (2.90), the first exponential term is a constant phase factor of no consequence, while the last is the carrier frequency. The middle exponential is a sinusoid of frequency $+2v/\lambda_t$, which is exactly the Doppler shift of Eq. (2.85). Thus the analysis approach of Eq. (2.87) is consistent with the earlier results.

In deriving Eq. (2.90), the time delay for the one-way propagation from the radar to the target has been effectively ignored; this assumption will be examined more closely in the next subsection. The approximation in going from the first line of Eq. (2.90) to the second is due to ignoring the term $2vt/c$ in the argument of the pulse envelope. This represents time compression of the envelope due to the moving target. In evaluating this term, the largest value of t that need be considered is the pulse length τ . The ratio of this time shift

to the pulse length is therefore $(2v\tau/c)/\tau = 2v/c$. Even for the fastest targets, this compression in the envelope duration is insignificant.

For a more interesting example of the use of Eq. (2.87), consider Fig. 2.18 again. Let a sidelooking radar be located at (x, y) coordinates $(x_r = 0, y_r = 0)$, and let the coordinates of the target aircraft be $(x_t = vt, y_t = R_0)$. This means that the target aircraft is initially directly abreast of the radar platform at a range R_0 at time $t = 0$, and is crossing orthogonal to the radar line of sight at a velocity v meters per second. The range between radar and aircraft is the Euclidean distance

$$\begin{aligned} R(t) &= \sqrt{R_0^2 + (vt)^2} \\ &= R_0 \sqrt{1 + \left(\frac{vt}{R_0}\right)^2} \end{aligned} \quad (2.91)$$

While it is possible to work with Eq. (2.91) directly, it is customary to expand the square root in a power series:

$$R(t) = R_0 \left[1 + \frac{1}{2} \left(\frac{vt}{R_0} \right)^2 - \frac{3}{8} \left(\frac{vt}{R_0} \right)^4 - \dots \right] \quad (2.92)$$

In evaluating this expression, the range of t that must be considered may be limited by any of several factors, such as the time the aircraft is within the radar main beam, or the coherent processing interval duration over which pulses will be collected for subsequent combining in the signal processor. In any event, it is almost always true that the distance traveled by the target within the time of interest vt is much less than the nominal range R_0 so that higher order terms can be neglected. Thus

$$R(t) \approx R_0 + \left(\frac{v^2}{2R_0} \right) t^2 \quad (2.93)$$

Equation (2.93) shows that the range is approximately a quadratic function of time for the crossing target scenario of Fig. 2.18. Using this truncated series in Eqs. (2.87) and (2.88) will give a result similar to Eq. (2.90)

$$\bar{y}(t) \approx a \left(t - \frac{2R_0}{c} \right) \exp \left(-j \frac{4\pi}{\lambda_t} R_0 \right) \exp \left[-j 2\pi \left(\frac{v^2}{R_0 \lambda_t} \right) t^2 \right] \exp(j 2\pi F_t t) \quad (2.94)$$

All of the terms are the same as in Eq. (2.90) except for the middle exponential. Because the phase function varies with the square of time, this is not a Doppler shift in the conventional sense of the term. Since instantaneous frequency is proportional to the time derivative of phase

$$F(t) = \frac{1}{2\pi} \frac{d\phi(t)}{dt} \quad (2.95)$$

this quadratic phase function represents a frequency component that varies linearly with time:

$$F_D(t) = -\frac{2v^2}{R_0\lambda_t}t \quad (2.96)$$

Thus, the “Doppler shift” of the received signal varies linearly due to the changing radar-target geometry. As the target aircraft approaches from the left in Fig. 2.18 ($t < 0$), the instantaneous Doppler shift is positive. When the aircraft is abreast of the radar ($t = 0$), the Doppler shift is zero because the radial component of velocity is zero. Finally, as the aircraft passes by the radar ($t > 0$), the Doppler shift becomes negative, as would be expected for a receding target.

This example shows how relative motion between radar and target can create time-varying Doppler shifts, and how the simple approach of Eq. (2.87) can be used to compute these shifts. The quadratic range case is important in synthetic aperture radar, and it will be revisited in Chap. 8 in more detail.

2.6.3 The “stop-and-hop” assumption and spatial Doppler

In this section, the model for an echo from a moving target is considered more closely. The one-way range from the radar to the target is again $R(t)$ along the line-of-sight axis, denoted here as the z axis. Suppose the transmitter is located at $z = 0$ and radiates the signal $\bar{x}(t)$ at time $t = 0$; the leading edge of the pulse is then at $z = ct$ at time t . The outgoing pulse will strike the target at some time t_1 such that $ct_1 = R(t_1)$. The echo will then be received another t_1 seconds later, so that the total two-way trip time is $t_d = 2t_1$. The echo received will simply be (ignoring amplitude scaling factors) a delayed replica of the transmitted signal

$$\bar{y}(t) = \bar{x}(t - t_d) \quad (2.97)$$

Consider again the constant velocity case where $R(t) = R_0 - vt$. The one-way travel time is given by

$$ct_1 = R_0 - vt_1 \Rightarrow t_1 = \frac{R_0}{c+v} \Rightarrow t_d = \frac{2R_0}{c+v} \quad (2.98)$$

Now consider the m th pulse in an M -pulse train. The result of Eq. (2.98) can be modified by assuming that the m th pulse is transmitted at time $t = mT$, where T is the radar PRI. The pulse and target are then located at z coordinates $c(t - mT)$ and $R_0 - vt = R_0 - vmT - v(t - mT)$ at time t . The one-way travel time after the pulse is transmitted is

$$t_1 = t - mT = \frac{R_0 - vmT}{c+v} \quad (2.99)$$

and the total round-trip delay t_d is twice this. It is convenient to form the following approximation to t_d

$$\begin{aligned} t_d &= \frac{2(R_0 - vmT)}{c + v} = \frac{2(R_0 - vmT)}{c(1 + \frac{v}{c})} \\ &= \frac{2(R_0 - vmT)}{c} \left[1 - \frac{v}{c} + \left(\frac{v}{c}\right)^2 - \dots \right] \\ &\approx \frac{2(R_0 - vmT)}{c} \left(1 - \frac{v}{c}\right) \end{aligned} \quad (2.100)$$

The transmitted signal for pulse m is

$$\bar{x}_m(t) = a(t - mT) \exp[j2\pi F_t(t - mT)] \quad (2.101)$$

and, using Eq. (2.100), the received signal becomes

$$\begin{aligned} \bar{y}_m(t) &= a\left(t - \frac{2(R_0 - vmT)}{c + v}\right) \exp\left[j2\pi F_t\left(t - \frac{2(R_0 - vmT)}{c + v}\right)\right] \\ &\approx a\left[t - mT - \frac{2(R_0 - vmT)}{c} \left(1 - \frac{v}{c}\right)\right] \\ &\quad \times \exp\left\{j2\pi F_t \left[t - mT - \frac{2(R_0 - vmT)}{c} \left(1 - \frac{v}{c}\right)\right]\right\} \\ &\approx a\left(t - mT - \frac{2(R_0 - vmT)}{c}\right) \\ &\quad \times \exp\left\{j2\pi F_t \left[t - mT - \frac{2(R_0 - vmT)}{c} \left(1 - \frac{v}{c}\right)\right]\right\} \end{aligned} \quad (2.102)$$

where the last line takes advantage of the fact that the additional time shift of the signal envelope due to the v/c term is insignificant.

Now sample this echo at a time delay after transmission that corresponds to the nominal range R_0 . The sampled echo is

$$\begin{aligned} \bar{y}_m\left(mT + \frac{2R_0}{c}\right) &= a\left(\frac{v}{c}mT\right) \exp\left[j2\pi F_t\left(\frac{2v}{c}mT\right)\left(1 - \frac{v}{c}\right)\right] \\ &= a\left(\frac{v}{c}mT\right) \exp\left[j\frac{4\pi v m T}{\lambda_t} \left(1 - \frac{v}{c}\right)\right] \\ &= a\left(\frac{v}{c}mT\right) \exp\left[j2\pi\left(\frac{2v}{\lambda_t}\right)mT\right] \exp\left[-j\frac{4\pi v^2 m T}{\lambda_t c}\right] \end{aligned} \quad (2.103)$$

Denote the maximum value of mT as the *aperture time*[†] T_a ; thus $T_a = (M - 1)T \approx MT$. The envelope term $a(vmT/c)$ is a constant equal to the

[†]This terminology is adopted from synthetic aperture imaging and will be explained in Chap. 8.

envelope amplitude so long as $vT_a < c\tau$, which states that the target motion during the aperture time T_a is less than the pulse span $c\tau$, that is, the target does not move more than a pulse length. This is normally the case for Doppler processing, which uses short aperture times. When synthetic aperture imaging is considered in Chap. 8, this condition may be violated, introducing the complication of *range migration*.

Now consider the two phase terms in Eq. (2.103). The first term is a discrete time complex sinusoid $\exp(j\omega m)$ with $\omega = 2\pi(2v/\lambda_t)T$, corresponding again to an analog Doppler frequency of $2v/\lambda_t$ hertz. The second term is another discrete sinusoid with a frequency of $-2v^2T/\lambda_t c$ hertz. It is more useful to consider the total phase excursion of this term. It is seen in Chap. 8 that this term has no significant impact on the spectrum of the measured data sequence provided that the maximum phase change over the aperture time is less than a fraction of π radians. Choosing a standard of $\pi/4$ and recalling that the maximum value of mT is no more than T_a , this requires that

$$\frac{4\pi v^2 T_a}{\lambda_t c} < \frac{\pi}{4} \Rightarrow T_a < \frac{\lambda_t c}{16v^2} \quad (2.104)$$

This inequality must be evaluated for any particular situation, but is easily satisfied for a vast majority of cases.[†] In this event, the received and sampled signal becomes simply

$$\bar{y}_m \left(mT + \frac{2R_0}{c} \right) = a \left(\frac{v}{c} mT \right) \exp \left[j 2\pi \left(\frac{2v}{\lambda_t} \right) mT \right] \quad (2.105)$$

Now repeat the development of Eqs. (2.99) through (2.103) under the assumption that there is no range change between the target and radar during the one-way travel time of a pulse. This will result in the $(c+v)$ term in Eq. (2.99) being replaced by simply c . This in turn will replace the $[1+(v/c)]$ terms with simply 1, and the model of the received signal will then be exactly that of Eq. (2.105). This assumption is often referred to as the *stop-and-hop assumption*. In synthetic aperture imaging, where the “target” is stationary ground scatterers, it effectively assumes that the radar, which is on a moving platform, stops and hovers as it transmits and receives each pulse, and then “hops” forward by vT meters before stopping to transmit the next pulse. In Doppler processing, where the target is moving and the radar platform may or may not be in motion, it is tantamount to assuming that both the target and radar stop during pulse transmission and reception, and then move the appropriate amounts during the pulse repetition interval before stopping for the next pulse. The stop-and-hop assumption allows the second phase term in Eq. (2.103) to be neglected, permitting use of the simple $2v/\lambda$ model for Doppler shift.

It was pointed out previously that typical values of Doppler shift are too small to be detected within a typical pulse length. How then is Doppler shift

[†]While almost always valid in radar, the stop-and-hop assumption is often not valid in sonar signal processing, requiring extra phase corrections in sonar Doppler processing and imaging not used in radar algorithms.

measured? Equation (2.105) showed that the sequence of coherent samples taken from the *same* range bin (same time delay $2R/c$ after pulse transmission) over multiple pulses forms a discrete-time sinusoid. The normalized radian frequency is $4\pi vT/\lambda_t$ radians, corresponding to $2v/\lambda_t$ hertz. Note that this series of samples is simply the slow-time sequence $y[l_0, m]$, where l_0 is the range bin corresponding to range R_0 . Thus, the phase progression of a slow-time data sequence for a range bin containing a moving target provides a measure of the Doppler shift of the target. The longer observation time T_a corresponding to having M pulses provides the resolution necessary to measure small Doppler shifts. Recall that it is assumed that the relationship between the target velocity, total observation time, and range bin spacing is such that the target remains within a single range bin over M pulses, i.e., for MT seconds.

The manifestation of the target Doppler in the slow-time phase progression is sometimes referred to as *spatial Doppler*. This terminology emphasizes the fact that the Doppler shift is measured not from intrapulse frequency changes, but rather from the change of absolute phase of the echoes at a given range bin over a series of pulses. Because of the inability to measure intrapulse Doppler frequency shifts in most systems, the term Doppler processing in radar refers to sensing and processing this spatial Doppler information. This concept extends to synthetic aperture imaging where, as shown previously, the Doppler shift is not constant.

2.7 Spatial Models

Previous sections have dealt with models of Doppler shift and the received power (both mean value and statistical fluctuations) of radar echoes from a single resolution cell. In this section, the variation in received power or complex voltage as a function of the spatial dimensions of range and angle will be considered. It will be seen that the observed complex voltage can be viewed as the output of a linear filter with the "true" variation in reflectivity over range or angle as its input. These relationships will lay the groundwork for an analysis of data sampling requirements and range and angle resolution in subsequent chapters.

Consider a stationary pulsed radar. On the m th pulse it transmits the equivalent complex signal.

$$\bar{x}(t; m) = \sqrt{P_t} x(t - t_m) \exp(j 2\pi F_t t) \quad (2.106)$$

In Eq. (2.106), $x(t)$ represents the modulation of the sinusoidal carrier, including both amplitude (typically on-off pulsing) and any phase modulation, and t_m is the time of transmission of the m th pulse. Assume that $x(t)$ has unit amplitude, so that the transmitted signal amplitude is represented by the term $\sqrt{P_t}$.

This signal echoes off a differential scatterer of cross section $d\sigma(R, \theta, \phi)$ at coordinates (R, θ, ϕ) . The corresponding differential contribution to the complex

voltage is, from Eq. (2.50), $d\xi(R, \theta, \phi) \exp[j\psi(R, \theta, \phi)]$, so that $d\sigma = |d\xi \exp(j\psi)|^2$.[†] The antenna may be scanning in either or both angle coordinates, so that at time t_m it is steered in the direction (θ_m, ϕ_m) . Then from Eq. (2.16) and (2.2) the differential received signal is

$$\begin{aligned} d\bar{y}(\theta_m, \phi_m, t - t_m; R, \theta, \phi) &= \sqrt{\frac{P_t P^2(\theta - \theta_m, \phi - \phi_m) \lambda^2}{(4\pi)^3 R^4 L_s L_a(R)}} d\xi(R, \theta, \phi) \dots \\ &\times \exp[j\psi(R, \theta, \phi)] x\left(t - t_m - \frac{2R}{c}\right) \exp\left[j2\pi F_t \left(t - \frac{2R}{c}\right)\right] \end{aligned} \quad (2.107)$$

Equation (2.107) can be simplified by separating the reflectivity terms and the terms which depend on spatial location, collapsing all of the other system-dependent amplitude terms into a single constant A_r . The term $d\xi \exp(j\psi)$ is termed the *baseband complex reflectivity* or just *reflectivity* of the differential scatterer, and will be denoted as $d\rho$. Making these substitutions gives

$$\begin{aligned} d\bar{y}(\theta_m, \phi_m, t - t_m; R, \theta, \phi) &= A_r d\rho(R, \theta, \phi) \left[\frac{P(\theta - \theta_m, \phi - \phi_m)}{\sqrt{L_a(R)} R^2} x\left(t - t_m - \frac{2R}{c}\right) \exp\left(j\frac{4\pi}{\lambda_t} R\right) \right] \\ &\times \exp(j2\pi F_t t) \end{aligned} \quad (2.108)$$

Coherent demodulation removes the carrier term, leaving only the baseband complex received voltage dy for the single differential scatterer

$$\begin{aligned} dy(\theta_m, \phi_m, t - t_m; R, \theta, \phi) &= A_r d\rho(R, \theta, \phi) \left[\frac{P(\theta - \theta_m, \phi - \phi_m)}{\sqrt{L_a(R)} R^2} x\left(t - t_m - \frac{2R}{c}\right) \exp\left(j\frac{4\pi}{\lambda_t} R\right) \right] \\ &\times \exp(j2\pi F_t t) \end{aligned} \quad (2.109)$$

Equation (2.109) gives the contribution to the received voltage of the echo of the m th pulse from a differential scatterer element at coordinates (R, θ, ϕ) . The total received voltage is obtained by integrating these differential contributions over all space:

$$y(\theta_m, \phi_m, t - t_m; R, \theta, \phi) = \int_{\phi=-\frac{\pi}{2}}^{\frac{\pi}{2}} \int_{\theta=-\pi}^{\pi} \int_{R=0}^{\infty} dy(\theta_m, \phi_m, t - t_m; R, \theta, \phi) \quad (2.110)$$

[†]The term involving ψ accounts for a possible constant phase shift on reflection at the scatterer surface.

Now write $d\rho(R, \theta, \phi) = \rho(R, \theta, \phi) dR d\theta d\phi$, $t'_m = t - t_m$ and use those results in Eq. (2.109) and (2.110) to obtain

$$\begin{aligned} y(\theta_m, \phi_m, t'_m; R, \theta, \phi) &= A_r \int_{\phi=\frac{\pi}{2}}^{\frac{\pi}{2}} \int_{\theta=-\pi}^{\pi} \int_{R=0}^{\infty} \left\{ \frac{\exp[j(4\pi/\lambda_t)R]}{\sqrt{L_a(R)}R^2} \rho(R, \theta, \phi) \right\} \dots \\ &\quad \times \left[P(\theta - \theta_m, \phi - \phi_m) x\left(t'_m - \frac{2R}{c}\right) dR d\theta d\phi \right] \end{aligned} \quad (2.111)$$

Define the *effective reflectivity* ρ' to include the amplitude modulation due to wave spreading and atmospheric loss, and also the phase rotation due to two-way propagation range

$$\rho'(R, \theta, \phi) = \frac{\exp[j(4\pi/\lambda_t)R]}{R^2 \sqrt{L_a(R)}} \rho(R, \theta, \phi) \quad (2.112)$$

Applying Eq. (2.112) to Eq. (2.111), the received signal is recognized as a *three-dimensional convolution* of the effective reflectivity with a convolution kernel comprising the antenna power pattern in the angle coordinates and the pulse modulation function in the range coordinate. Specifically

$$y(\theta_m, \phi_m, t'_m) = A_r \rho'(ct'_m/2, \theta_m, \phi_m) *_{t'_m} *_{\theta_m} *_{\phi_m} [P(-\theta_m, -\phi_m) x(t'_m)] \quad (2.113)$$

where the symbols $*_{t'_m}$, $*_{\theta_m}$, and $*_{\phi_m}$ denote convolution over the indicated coordinate. Now assume the antenna pattern is symmetric in the two angular coordinates, as is often the case; rescale the time variable to units of range; and replace θ_m and ϕ_m with general angular variables θ and ϕ . These substitutions finally give

$$y(\theta, \phi, R) = A_r \rho'(R, \theta, \phi) *_R *_\theta *_\phi \left[P(\theta, \phi) x\left(\frac{2R}{c}\right) \right] \quad (2.114)$$

Strictly speaking, Eq. (2.111) can be interpreted as the three-dimensional convolution of Eq. (2.114) only with the aid of some additional assumptions. These are discussed in Sec. 2.7.1 and 2.7.2, but do not detract from our main argument.

Equation (2.114) is a fundamental result. It shows that the transmitted waveform and antenna power pattern act as linear filters in the range and angle coordinates, respectively. The observed reflectivity distribution, as represented by the receiver output voltage, is a filtered and weighted version of the actual reflectivity distribution. The range resolution of the reflectivity function is therefore limited by the pulse modulation function $x(t)$ while the angular resolution is limited by the antenna beamwidth. Since most pulsed radars use pulse lengths between perhaps 50 ns and 100 μ s, the corresponding range resolution of the measured reflectivity profile varies from 7.5 m to 15 km and is determined by the pulse length. (In Chap. 4 it will be seen that the introduction of matched filtering will significantly change this statement.) Antennas have been designed for a wide range of beamwidths, with the higher resolution

“pencil beam” antennas typically between $1/3^\circ$ and 10° beamwidths. The corresponding angular resolution in meters is usually coarser than the range resolution, and furthermore increases with range. (In Chap. 7 it will be seen that the introduction of synthetic aperture techniques also significantly changes this statement.)

It also follows from the filtering action of $x(t)$ and $P(\theta, \phi)$ that the bandwidth of the measured reflectivity function is limited by the bandwidth of the waveform modulation function and antenna power pattern. This observation will be used in Chap. 3 to determine the range and angle sampling requirements.

2.7.1 Variation with angle or cross-range

Now consider the variation in reflectivity with angle for a fixed range, say R_0 . Define the range-averaged effective reflectivity

$$\begin{aligned}\hat{\rho}(\theta, \phi; R_0) &= \int_R x \left[\frac{2}{c} (R_0 - R) \right] \rho'(R, \theta, \phi) \\ &= \left[\rho'(R, \theta, \phi) *_R x \left(\frac{2R}{c} \right) \right]_{R=R_0}\end{aligned}\quad (2.115)$$

This is the reflectivity variation in angle, taking into account the range averaging at each angle due to the finite pulse length. Note that in the limit of very fine range resolution, i.e., if the pulse modulation $x(2R/c) \rightarrow \delta_D(R - R_0)$, then $\hat{\rho}(\theta, \phi; R_0) \rightarrow \rho'(R_0, \theta, \phi)$, that is, the “range-averaged” reflectivity would exactly equal the effective reflectivity evaluated at the range of interest R_0 .

Applying Eq. (2.115) to Eq. (2.114) gives

$$\begin{aligned}y(\theta, \phi; R_0) &= A_r \int_{\xi=-\frac{\pi}{2}}^{\frac{\pi}{2}} \int_{\zeta=-\pi}^{\pi} P(\zeta - \theta, \xi - \phi) \hat{\rho}(\theta, \phi; R_0) d\xi d\zeta \\ &= \hat{\rho}(\theta, \phi; R_0) *_{\theta} *_{\phi} P(\theta, \phi)\end{aligned}\quad (2.116)$$

where again symmetry of the antenna pattern has been assumed in the second line. Equation (2.116) is a special case of Eq. (2.114) showing that the complex voltage at the output of a coherent receiver for a fixed range and a scanning antenna is the convolution in the angle dimensions of the range-averaged effective reflectivity function evaluated at the range R_0 , $\hat{\rho}(\theta, \phi; R_0)$, with the antenna power pattern $P(\theta, \phi)$.

As mentioned earlier, some care must be taken in interpreting the relation of Eq. (2.116) as a convolution. Suppose that the elevation angle ϕ is fixed, and consider only the variation in azimuth angle θ . Because the integration is over a full 2π radians and the integrand is periodic in θ with period 2π , the integration over azimuth is a true convolution of periodic functions.

This would not appear to be the case if instead θ is fixed and ϕ varies because the integrand is over a range of only π radians. However, one could equally well

write Eq. (2.116) as

$$\begin{aligned} y(\theta, \phi; R_0) &= A_r \int_{\xi=-\pi}^{\pi} \int_{\zeta=-\frac{\pi}{2}}^{\frac{\pi}{2}} P(\xi - \theta, \zeta - \phi) \hat{\rho}(\theta, \phi; R_0) d\xi d\zeta \\ &= \hat{\rho}(\theta, \phi; R_0) *_{\theta} *_{\phi} P(\theta, \phi) \end{aligned} \quad (2.117)$$

For fixed azimuth, this is now a convolution of periodic functions in elevation. Taken together, there is a two-dimensional averaging over the (θ, ϕ) space. Finally, note that Eq. (2.116) can be recast from angle units into units of cross range X and Y using the transformations $X = R_0\theta$ and $Y = R_0\phi$:

$$y(X, Y; R_0) = A_r \int_{X=-\frac{\pi R}{2}}^{\frac{\pi R}{2}} \int_{Y=-\pi R}^{\pi R} P\left[\frac{1}{R_0}(X - \alpha, Y - \beta)\right] \hat{\rho}\left(\frac{X}{R_0}, \frac{Y}{R_0}; R_0\right) d\alpha d\beta \quad (2.118)$$

Figure 2.19 illustrates intuitively in one angle dimension the process described by Eq. (2.116). Assume that the elevation angle is fixed at $\phi = 0^\circ$ and consider only the azimuth variation. An array of ideal point scatterers is illuminated by a radar that scans in azimuth across the target field. The response to any one scatterer is maximum when the radar boresight is aimed at that scatterer; as the radar boresight moves away, the strength of the echo declines because less energy is directed to the scatterer on transmission, and the antenna is also less sensitive to echoes from directions other than the bore-sight on reception. For an isolated scatterer, the amplitude of the coherent baseband received signal $y(\theta, 0; R_0)$ at the receiver output will be proportional

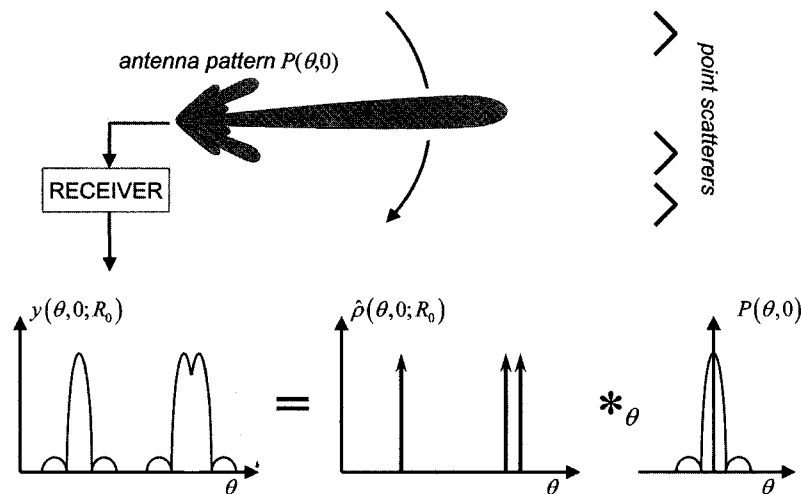


Figure 2.19 When scanning past an array of point scatterers, the receiver output is a superposition of replicas of the antenna pattern.

to $P(\theta, 0)$. Thus, a graph of the received signal mimics the antenna azimuth pattern.

Assuming a linear receiver so that superposition applies, the response to two closely spaced point scatterers is proportional to two replicas of the antenna pattern, overlapped and added to get a composite response. If the two scatterers are close enough together, the individual responses are not resolved, but instead blur together into a single peak as illustrated in Fig. 2.19. Clearly, the separation at which scatterers are resolved depends on the antenna pattern $P(\theta, 0)$.

The spatial Fourier transform of the observed signal is the input spatial Fourier transform multiplied by the Fourier transform of the antenna pattern. Practical antenna patterns have lowpass spectra. Equation (2.119) gives the ideal two-way azimuth voltage patterns for circular and rectangular apertures of width D (Balanis, 1982):

$$\begin{aligned} P(\theta, 0) &= \left[\frac{J_1(\pi D \sin \theta / \lambda)}{\pi D \sin \theta / \lambda} \right]^2 && \text{(circular aperture)} \\ P(\theta, 0) &= \left[\frac{\sin(\pi D \sin \theta / \lambda)}{\pi D \sin \theta / \lambda} \right]^2 && \text{(rectangular aperture)} \end{aligned} \quad (2.119)$$

Figure 2.20 plots these patterns on a decibel scale for the case $D = 40\lambda$.

The corresponding spatial spectra are shown in Fig. 2.21; for the rectangular aperture, it is a triangle function with a support of twice the aperture width. The reason is easy to see: the one-way voltage pattern is just the inverse Fourier transform of the aperture function, which for uniform illumination is a rectangular pulse of the width of the aperture. When that pattern is squared to get the two-way pattern, the Fourier transform of the squared pattern is the self-convolution of the Fourier transform of the unsquared pattern. Thus, the rectangular aperture function is convolved with itself to give a triangle of twice the aperture width. The spectrum for the circular aperture has the same width but is somewhat smoother.

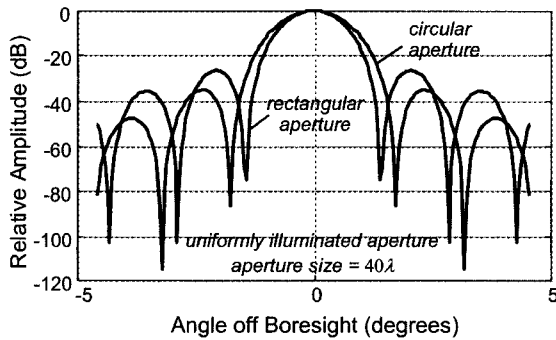


Figure 2.20 Two-way antenna gain patterns for ideal, uniformly illuminated circular and rectangular apertures.

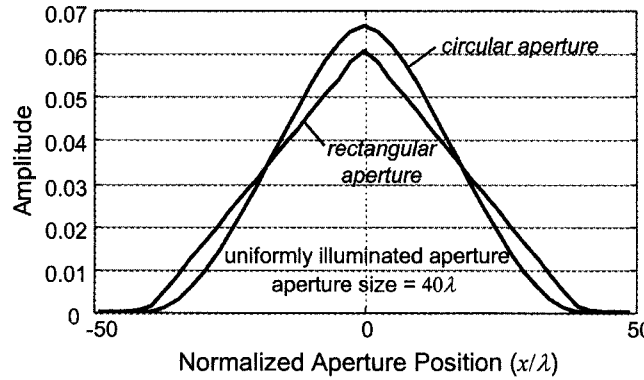


Figure 2.21 Spatial spectra corresponding to the antenna patterns of Fig. 2.20.

The spatial spectra of these idealized, but typical, antenna patterns are lowpass functions. Thus, the upper frequencies in the spatial spectrum of the observed data will be strongly attenuated and in fact effectively removed. Since resolution is proportional to bandwidth, Eq. (2.118) and Fig. 2.21 show that the antenna pattern reduces resolution because it has a strongly low-pass spatial spectrum.

2.7.2 Variation with range

A development similar to that in Sec. 2.7.1 can be carried out to specialize Eq. (2.115) for the variation of received voltage in the range dimension along the boresight look direction (θ_m, ϕ_m) .[†] First interchange the order of integration in Eq. (2.111) so that the outer integral is over range. Next, define the new quantity

$$\begin{aligned}\tilde{\rho}(R; m) &= \iint_{\theta, \phi} P(\theta - \theta_m, \phi - \phi_m) \rho'(R, \theta, \phi) d\theta d\phi \\ &= \rho'(R, \theta, \phi) *_{\theta} *_{\phi} P(\theta, \phi)|_{\theta=\theta_m, \phi=\phi_m}\end{aligned}\quad (2.120)$$

This is the reflectivity variation in range, taking into account the azimuth and elevation averaging at each range due to the nonideal antenna power pattern. Note that in the limit as the antenna power pattern tends to the ideal $P(\theta, \phi) \rightarrow G\delta_D(\theta, \phi)$, then $\tilde{\rho}(R; m) \rightarrow \rho'(R, \theta_m, \phi_m)$, that is, the “angle-averaged” reflectivity exactly equals the effective reflectivity along the antenna look direction, as expected.

[†]The analysis can be carried out equally easily for an off-boresight look direction. The only difference is to substitute an antenna gain value other than the peak gain G .

Applying Eq. (2.120) to Eq. (2.113) leaves (Munson and Visentin, 1989)

$$\begin{aligned} y\left(\frac{2R}{c}; m\right) &= A_r \tilde{\rho}(R; m) *_R \left[x\left(\frac{2R}{c}\right) \right] \\ &= A_r \int_{R'=0}^{\infty} x\left[\frac{2}{c}(R - R')\right] \tilde{\rho}(R'; m) dR' \end{aligned} \quad (2.121)$$

or an equivalent equation, using time units instead of range units

$$\begin{aligned} y(t; m) &= A_r \tilde{\rho}\left(\frac{ct}{2}; m\right) *_t [x(t)] \\ &= A_r \int_{t'=0}^{\infty} x(t' - t) \tilde{\rho}\left(\frac{ct'}{2}; m\right) dt' \end{aligned} \quad (2.122)$$

Equation (2.121) or (2.122), which are simply special cases of Eq. (2.113), make clear that the complex voltage at the output of a coherent receiver is the convolution in the range dimension of the angle-averaged effective reflectivity function in the radar look direction, $\tilde{\rho}(R; m)$ with the waveform modulation function $x(t)$.

Equation (2.112) expressed the relationship between the amplitude of the effective reflectivity ρ' and the actual reflectivity ρ resulting from weighting due to atmospheric loss and R^2 spreading. Whether this term is significant depends on the ratio of the maximum and minimum ranges of interest. For example, if a surveillance radar is mapping a 20-km swath between 80 and 100 km range, the variation in the R^2 term over the swath is only 1.94 dB. While significant, this is probably much less than the variations in ρ itself and may often be ignored. On the other hand, a millimeter wave seeker searching a footprint from 1 to 3 km downrange sees a variation of 9.54 dB in this term, which can probably not be ignored. In either case, the variation in amplitude due to R^2 is predictable and can be compensated in the signal processor by applying a range-dependent gain to the data. The compensation can be applied as the data are received by using a rapidly time-varying gain proportional to t^2 . This procedure is called *sensitivity time control* (STC). Alternatively, the correction can be applied in the signal or data processor.

The R^2 voltage gain (equivalent to R^4 power gain) correction assumes a range dependence of the received voltage corresponding to the point target form of the radar range equation (Eq. (2.19)). If the radar is illuminating a volume or area scatterer, a different correction factor is required because of the different range dependence of the received power. Thus, for volume scatterers or beam-limited area scatterers (Eq. (2.25) or (2.30)) the *voltage* gain should be varied as R , while for pulse-limited area scatterers Eq. (2.31) the voltage gain should be varied as $R^{3/2}$.

2.7.3 Projections

The range-averaged reflectivity $\hat{\rho}(\theta, \phi; R_0)$ of Eq. (2.115) and the angle-averaged reflectivity $\tilde{\rho}(R; m)$ of Eq. (2.120) are examples of *projections*. In each

case, the three-dimensional reflectivity is reduced in dimension by integrating over one or more dimensions. The angle-averaged reflectivity is reduced to a two-dimensional function by integrating over range, while the range-averaged reflectivity is reduced to a one-dimensional function by integrating over both angle coordinates.

The idea of projections, particularly the angle-averaged projection $\tilde{\rho}(R; m)$, will be important in deriving the polar format spotlight SAR algorithm in Chap. 8. The projections that will be needed are integrals over straight lines or planar surfaces. The averaging in Eq. (2.120) is over the surface of a sphere. However, for small beamwidths only a region of θ_3 radians in azimuth and ϕ_3 radians in elevation contributes significantly to the integral, and at long ranges this limited region is nearly planar.

2.7.4 Multipath

The convolutional model of the measured range profile is based on the assumption of superposition of backscattered fields and a one-to-one mapping of echo arrival time to range (Eq. (2.107)). The superposition of electric fields is a valid assumption while the mapping of time to range may not be. To illustrate, consider Fig. 2.22, which diagrams two phenomena that violate this assumption. Figure 2.22a illustrates the problem of *multipath*, in which echoes from the same target arrive at the radar receiver via two different paths. The first is the direct path of total length $2R_0$. The second is the “multipath” or “ground bounce” path with length $R_0 + R_1 + R_2 > 2R_0$. Though not shown,

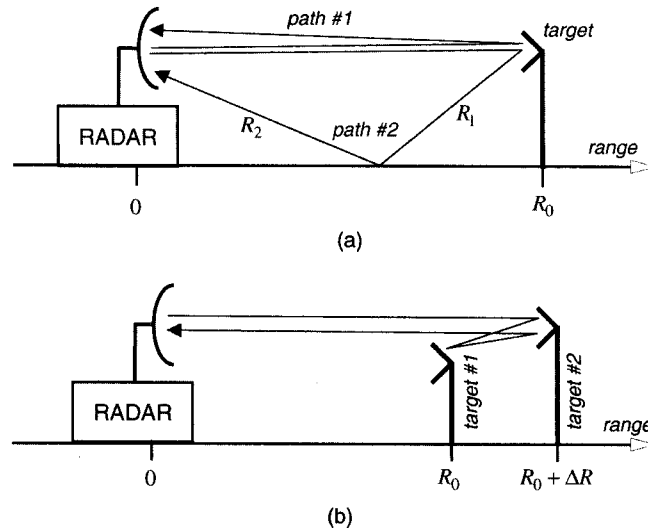


Figure 2.22 Illustration of two multiple-bounce scattering phenomena which violate the one-to-one mapping of time to range.

it is also possible for a portion of the transmitted wave to arrive at the target via the ground bounce and be scattered back along both of the paths in Fig. 2.22a, meaning that there may also be an echo with a time delay corresponding to a two-way path length of $2(R_0 + R_1 + R_2)$. Consequently, one scatterer may produce echoes at three different apparent ranges if multipath is present. Whether these appear as distinct echoes depends on the relationship between the path length difference and the pulse length. The ground bounce echoes are often, but not always, significantly attenuated with respect to the direct path echo. The degree of attenuation depends on the bistatic scattering characteristics of the surface, the antenna pattern characteristics (because the multipath bounce is not on the peak of the main lobe) and the problem geometry. As the range between target and radar varies, the path length difference also varies, so that the direct and multipath bounces may alternately add in and out of phase, provided the path length difference is such that the two received echoes overlap. Multipath is generally most significant for targets located at low altitude over a good reflecting surface such as a relatively smooth terrain or calm ocean and at long range, so that the grazing angles involved are small.

Figure 2.22b illustrates the effect of *multiple bounce* echoes in a situation involving two scatterers. A portion of the energy reflected from the more distant scatterer bounces off the nearer scatterer, then reflects a second time off the distant scatterer and returns to the radar. Obviously additional multiple bounces are also possible. For the situation sketched, three apparent echoes will again result, with the third due to a phantom scatterer $2\Delta R$ behind the second actual scatterer. As with multipath, the amplitude of multiple bounce echoes often falls off rapidly, and the same considerations of in- and out-of-phase superposition apply.

These possible differences in the measured and actual reflectivity distributions do not mean that range profile measurements are not useful. They do mean that in situations where significant multipath or multiple bounce phenomena are possible, the range profiles must be interpreted with care.

2.8 Spectral Model

There is one more interpretation of the received radar signal that proves useful in subsequent chapters. The preceding two sections have emphasized linear filtering models of the spatial reflectivity distribution as observed through the received complex baseband signals. However, it was pointed out previously that radar cross section is a function of, among many other things, the radar frequency. Thus, it is useful to investigate the significance of the radar transmitted frequency F_t on the reflectivity measurements.

To understand the role of transmitted frequency, it is necessary to deal with the radar signal while it is still at the radar frequency F_t . If the development from Eq. (2.106) to Eq. (2.122) is repeated without demodulating the signals to baseband and the range variation is considered, the RF version of Eq. (2.122)

can be obtained

$$\begin{aligned}\bar{y}(t; m) &= A_r \int_{t=0}^{\infty} x(t' - t) \tilde{\rho} \left(\frac{ct'}{2}; m \right) \exp(j 2\pi F_t t') dt' \\ &= A_r \left[\tilde{\rho} \left(\frac{ct}{2}; m \right) \exp(j 2\pi F_t t) \right] *_t [x(t)]\end{aligned}\quad (2.123)$$

Now consider the Fourier transform of $\bar{y}(t; m)$ with respect to the time (range) variable t . Using simple properties of Fourier transforms gives

$$\bar{Y}(F; k) = \frac{2A_r}{c} X(F) \tilde{P} \left[\frac{2(F - F_t)}{c} \right] \quad (2.124)$$

Figure 2.23 provides a pictorial interpretation of this equation under the assumption that the transmitted waveform $x(t)$ is a narrowband waveform. In this case,

$$\bar{Y}(F; k) \approx \frac{2A_r}{c} \tilde{P} \left(\frac{-2F_t}{c} \right) X(F) \quad (2.125)$$

so that the amplitude of the spectrum of the received pulse, and therefore of the pulse itself, is proportional to the amplitude of the spectrum of the angle averaged range profile, evaluated at the transmitted frequency. Since it is the complex spectrum that appears in Eq. (2.125), both the amplitude and phase of the returned pulse are affected by the amplitude and phase of the reflectivity spectral sample.

Equation (2.125) shows that a narrowband radar pulse can be interpreted as measuring a frequency sample of the spectrum of the angle-averaged reflectivity range variation. This concept is important in understanding the behavior of frequency stepped radars in Chap. 4.

Another case of interest occurs when $x(t)$ is a wideband pulse. In this case, the spectrum $X(F)$ is approximately a rectangle as shown in Fig. 2.24. The spectrum of the receiver waveform $\bar{y}(t; m)$ is then approximately that of the

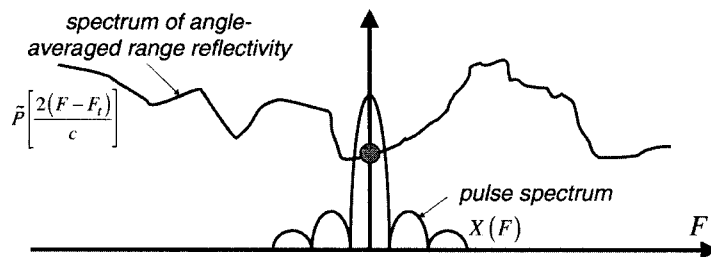


Figure 2.23 Pictorial interpretation of Eq. (2.124), illustrating the spectral windowing effect of a narrowband radar pulse.

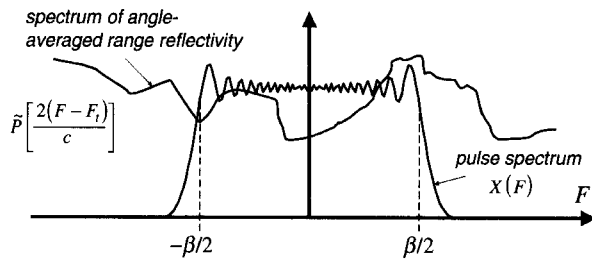


Figure 2.24 Pictorial interpretation of Eq. (2.124) illustrating the spectral sampling effect of a wideband radar pulse.

angle-averaged range profile over the bandwidth of the pulse

$$\tilde{Y}(F; m) \approx \frac{2A_r}{c} \tilde{P}\left[\frac{2(F - F_t)}{c}\right] \quad -\frac{\beta}{2} \leq F \leq +\frac{\beta}{2} \quad (2.126)$$

In other words, the pulse spectrum acts as a window selecting a portion of the spectrum of the angle-averaged reflectivity. This result will be useful in understanding the use of linear FM and other modulated waveforms to achieve high range resolution in Chap. 4.

2.9 Summary

An understanding of the nature of the signals of interest is prerequisite to the design of successful signal processing systems. This chapter reviews the most common signal models used in designing and analyzing radar signal processors. It has been seen that multiple views of the radar echo are used: its variation in amplitude, space, time, and frequency, and deterministic and statistical interpretations of these variations.

Radar signal modeling traditionally focuses most strongly on amplitude models, that is, on radar cross section. RCS is viewed as a deterministic quantity, predictable in principle through the use of Maxwell's equations if the scattering is modeled accurately enough. The radar range equation in its many forms (only a very small subset of which has been introduced here) is the radar engineer's most fundamental tool for estimating received signal amplitude or, conversely, determining required system characteristics such as transmitted power or antenna gain.

The radar system is a measuring instrument, used to observe the variation of RCS in space. Its pulse function (modulation and carrier term) and antenna power pattern determine its measurement characteristics, which in turn determine the achievable resolution and required sampling rates. The effect of the radar measurement system on the spatial variation of observed RCS is well-modeled by the convolution of the combined pulse-and-antenna pattern measurement kernel with the three-dimensional reflectivity function.

This important observation means that the tools of linear systems analysis can be brought to bear to help analyze and understand the performance of radar systems. The carrier frequency, in combination with any Doppler shifts, determines what portion of the reflectivity frequency spectrum is sampled by the pulse. This observation reinforces the need for frequency domain analyses of radar measurements. Linear systems and frequency domain viewpoints are relied on heavily throughout the remainder of the book.

Even though RCS is a deterministic quantity, its sensitivity to radar frequency, aspect angle, and range coupled with the complexity of typical targets results in very complex behavior of observed amplitude measurements. Statistical models are used to describe this complexity. A variety of statistical models, comprising both probability density functions and correlation properties, have gained acceptance for various scenarios and form the basis for much analysis, particularly in calculations of probabilities of detection and false alarm, two of the most important radar performance measures.

References

- Balanis, C. A., *Antenna Theory*. Harper & Row, New York, 1982.
- Baxa, E. G., Jr., "Airborne Pulsed Doppler Radar Detection of Low-Altitude Windshear-A Signal Processing Problem," *Digital Signal Processing*, vol. 1, no. 4, pp. 186–197, Oct. 1991.
- Beckmann, P., and A. Spizzichino, *The Scattering of Electromagnetic Waves from Rough Surfaces*. MacMillan, New York, 1963.
- Birkmeier, W. P., and N. D. Wallace, *AIEE Transactions on Communication Electronics*, vol. 81, pp. 571–575, Jan. 1963.
- Carlson, A. B., *Communication Systems*. McGraw-Hill, New York, 1976.
- Curlander, J. C., and R. N. McDonough, *Synthetic Aperture Radar*. Wiley, New York, 1991.
- Currie, N. C., "Clutter Characteristics and Effects," Chap. 10 in J. L. Eaves and E. K. Reedy (eds.), *Principles of Modern Radar*. Van Nostrand Reinhold, New York, 1987.
- Doviak, D. S., and R. J. Zrnic, *Doppler Radar and Weather Observations*, 2d ed. Academic Press, San Diego, CA, 1993.
- Eaves, J. L., and E. K. Reedy, *Principles of Modern Radar*. Van Nostrand Reinhold, New York, 1987.
- Gill, T. P., *The Doppler Effect*. Logos Press, London, 1965.
- Haykin, S., B. W. Currie, and S. B. Kesler, "Maximum Entropy Spectral Analysis of Radar Clutter," *Proceedings of the IEEE*, vol. 70, no. 9, pp. 953–962, Sept. 1982.
- Holm, W. A., "MMW Radar Signal Processing Techniques," Chap. 6 in N. C. Currie and C. E. Brown (eds.), *Principles and Applications of Millimeter-Wave Radar*. Artech House, Boston, MA, 1987.
- Jakeman, E., and P. N. Pusey, "A Model for Non-Rayleigh Sea Echo," *IEEE Transactions on Antennas and Propagation*, vol. 24, no. 6, pp. 806–814, Nov. 1976.
- Kay, S. M., *Modern Spectral Estimation*. Prentice Hall, Englewood Cliffs, NJ, 1988.
- Knott, E. F., J. F. Shaeffer, and M. T. Tuley, *Radar Cross Section*. Artech House, Boston, MA, 1985.
- Levanon, N., *Radar Principles*. Wiley, New York, 1988.
- Lewinski, D. J., "Nonstationary Probabilistic Target and Clutter Scattering Models," *IEEE Transactions on Antennas and Propagation*, vol. AP-31, no. 3, pp. 490–498, May 1983.
- Long, M. W., *Radar Reflectivity of Land and Sea*, 3d ed. Artech House, Boston, MA, 2001.
- Lothes, R. N., M. B. Szymanski, and R. G. Wiley, *Radar Vulnerability to Jamming*. Artech House, Boston, MA, 1990.
- Meyer, D. P., and H. A. Mayer, *Radar Target Detection*. Academic Press, New York, 1973.
- Mott, H., *Polarization in Antennas and Radar*. Wiley, New York, 1986.
- Munson, D. C., and R. L. Visentin, "A Signal Processing View of Strip-Mapping Synthetic Aperture Radar," *IEEE Transactions on Acoustics, Speech, and Signal Processing*, vol. 27, no. 12, pp. 2131–2147, 1989.
- Nathanson, F. E., *Radar Design Principles*, 2d ed. McGraw-Hill, New York, 1991.

-
- Omura, J., and T. Kailath, "Some Useful Probability Distributions," Technical Report No. 7050-6, Stanford Electronics Laboratories, Stanford University, Sep. 1965. Also identified as report no. SU-SEL-65-079.
- Papoulis, A., *Probability, Random Variables, and Stochastic Processes*, 2d ed. McGraw-Hill, New York, 1984.
- Probert-Jones, J. R., "The Radar Equation in Meteorology," *Quarterly Journal of the Royal Meteorological Society*, vol. 88, pp. 485-495, 1962.
- Ray, H., "Improving Radar Range and Angle Detection with Frequency Agility," *Microwave Journal*, p. 64ff, May 1966.
- Sangston, K. J., "Toward a Theory of Ultrawideband Sea Scatter," *Proceedings of IEEE National Radar Conference*, pp. 160-165, 1997.
- Sauvageot, H., *Radar Meteorology*. Artech House, Boston, MA, 1992.
- Skolnik, M. I., *Introduction to Radar Systems*, 3d. ed. McGraw-Hill, New York, 2001.
- Swerling, P., "Probability of Detection for Fluctuating Targets," *IRE Transactions on Information Theory*, vol. IT-6, pp. 269-308, April 1960.
- Temes, C. L., "Relativistic Consideration of Doppler Shift," *IRE Transactions on Aeronautical and Navigational Electronics*, p. 37, 1959.
- Ulaby, F. T., and M. C. Dobson, *Handbook of Radar Scattering Statistics for Terrain*. Artech House, Norwood, MA, 1989.
- Ward, K. D., "Compound Representation of High Resolution Sea Clutter," *Electronics Letters*, vol. 17, no. 16, pp. 561-563, Aug. 6, 1981.
- Ziemer, R. E., and W. H. Tranter, *Principles of Communications*. Houghton Mifflin, Boston, MA, 1976.



3

Sampling and Quantization of Pulsed Radar Signals

3.1 Domains and Criteria for Sampling Radar Signals

As has been seen, a radar measures the spatial distribution of reflectivity in the three-dimensional spherical coordinate system of range, azimuth angle, and elevation angle. Many radars also process the signals in domains corresponding to the Fourier transform of either slow-time (pulse number) or, in the case of array antennas, receiver channel. These spectral domains correspond to Doppler shift and angle of arrival, respectively, and represent the fourth and fifth potential dimensions of a radar signal. If the signals are to be processed digitally, one of the first questions to arise is how the sampling interval should be chosen in each dimension.

A pulsed radar has several distinct and independent sampling intervals; six are identified here. The first two are both time sampling intervals. Consider Fig. 3.1, which illustrates the general data collection strategy of a pulsed radar, possibly with a multi-phase center antenna such as a phased array. The radar emits a periodic series of pulses; the period is denoted as the *pulse repetition interval* (PRI), and its inverse is the *pulse repetition frequency* (PRF).[†] The PRF may range from a few hundred hertz to tens and sometimes a few hundreds of kilohertz. In a portion of the time period between pulses, the received signal from each antenna channel is sampled at a high rate, typically in the range of hundreds of kilohertz to a few tens of megahertz, and sometimes higher. After conversion to baseband, the cluster of high rate samples from one channel and one pulse may be viewed as being stored in a single row and layer of the

[†]In this text, the abbreviation “PRF” is used both as an acronym and as a mathematical variable. When used as an acronym, it is not italicized (PRF); when used as a mathematical variable, it is italicized (*PRF*).